

Iron Complexes Derived from $\{\text{nacnac}(\text{CH}_2\text{py})_2\}^-$ and $\{\text{nacnac}(\text{CH}_2\text{py})(\text{CHpy})\}^n$ Ligands: Stabilization of Iron(II) via Redox Noninnocence

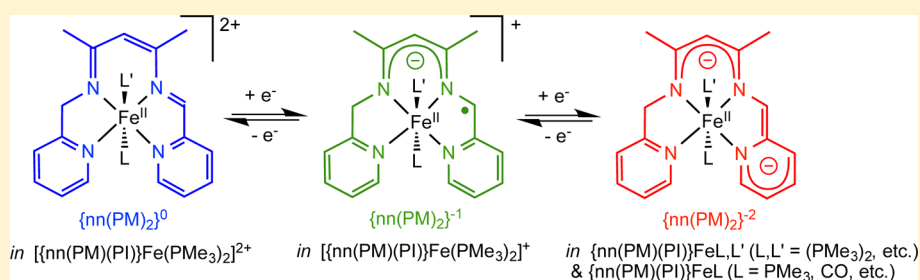
Valerie A. Williams,[†] Peter T. Wolczanski,^{*,†} Jörg Sutter,[‡] Karsten Meyer,[‡] Emil B. Lobkovsky,[†] and Thomas R. Cundari[§]

[†]Baker Laboratory, Department of Chemistry & Chemical Biology, Cornell University, Ithaca, New York 14853, United States

[‡]Department of Chemistry & Pharmacy, University of Erlangen-Nuremberg, Egerlandstrasse 1. D-91058 Erlangen, Germany

[§]Department of Chemistry, Center for Advanced Scientific Computing and Modeling (CASCAM), University of North Texas, Box 305070, Denton, Texas 76203-5070, United States

Supporting Information



ABSTRACT: Nacnac-based tetradentate chelates, $\{\text{nacnac}(\text{CH}_2\text{py})_2\}^-$ ($\{\text{nn}(\text{PM})_2\}^-$) and $\{\text{nacnac}(\text{CH}_2\text{py})(\text{CHpy})\}^n$ ($\{\text{nn}(\text{PM})(\text{PI})\}^n$) have been investigated in iron complexes. Treatment of $\text{Fe}\{\text{N}(\text{TMS})_2\}_2(\text{THF})$ with $\{\text{nn}(\text{PM})_2\}\text{H}$ afforded $\{\text{nn}(\text{PM})_2\}\text{FeN}(\text{TMS})_2$ [**1-N**(TMS)₂], which led to $\{\text{nn}(\text{PM})_2\}\text{FeCl}$ (**1-Cl**) from HCl and to $\{\text{nn}(\text{PM})_2\}\text{FeN}_3$ (**1-N₃**) upon salt metathesis. Dehydroamination of **1-N**(TMS)₂ was induced by L (L = PMe₃, CO) to afford $\{\text{nn}(\text{PM})(\text{PI})\}\text{Fe}(\text{PMe}_3)_2$ [**2-(PMe₃)₂**] and $\{\text{nn}(\text{PM})(\text{PI})\}\text{FeCO}$ (**3-CO**). Substitution of 2-(PMe₃)₂ led to $\{\text{nn}(\text{PM})(\text{PI})\}\text{Fe}(\text{PMe}_3)\text{CO}$ [**2-(PMe₃)CO**], and exposure to a vacuum provided $\{\text{nn}(\text{PM})(\text{PI})\}\text{Fe}(\text{PMe}_3)$ (**3-PMe₃**). Metathesis routes to $\{\text{nn}(\text{PM})(\text{PI})\}\text{FeL}_2$ (**2-L₂**; L = PMe₃, PMe₂Ph) and $\{\text{nn}(\text{PM})(\text{PI})\}\text{FeL}$ (**3-L**; L = PMePh₂, PPh₃) from [$\{\text{nn}(\text{PM})(\text{PI})\}^{2-}$]₂Li₂ and FeBr₂(THF)₂ in the presence of L proved feasible, and 1e⁻ and 2e⁻ oxidation of 2-(PMe₃)₂ afforded 2⁺-(PMe₃)₂ and 2²⁺-(PMe₃)₂ salts. Mössbauer spectroscopy, structural studies, and calculational assessments revealed the dominance of iron(II) in both high-spin (**1-X**) and low-spin (**2-L₂** and **3-L**) environments, and the redox noninnocence (RNI) of $\{\text{nn}(\text{PM})(\text{PI})\}^n$ [**2-L₂**, **3-L**, n = 2⁻; 2⁺-(PMe₃)₂, n = 1⁻; 2²⁺-(PMe₃)₂, n = 0]. A discussion regarding the utility of RNI in chemical reactivity is proffered.

1. INTRODUCTION

In recent studies pertaining to first-row complexes containing the di-2-pyridyl-2-azaallyl (smif) ligand and variants,^{1–6} various C–C bond-making reactions have been discovered.^{3–6} A fully occupied orbital localized primarily on the azaallyl functionality is essentially nonbonding (i.e., CNC^{nb}) and can be considered to have either diradical or ionic character. In concert with this description, azaallyl fragments display reactivity that can be construed as radical couplings or bond formation via complementary nucleophilic/electrophilic paths.

Selected examples of the type of reactivity observed for the azaallyl precursors are illustrated in Figure 1, where the ambiguity in the mode of C–C bond formation persists. For instance, in **A**, the simple, reversible backbone coupling found for the dimerization of (smif)FeN(TMS)₂ is consistent with diradical coupling,^{3,6} but the reaction may also be viewed as a mutual attack by nucleophilic carbon atoms of each backbone on the remaining electrophilic carbon atoms. The C–C bond

formation in **B** appears to be a related radical coupling of two smif azaallyls that span two iron centers.⁶ Ferrous centers that result from the coupling are accompanied by two PI radical anions, rendering the mechanistic assessment tentative, because plausible disproportionation paths provide a surfeit of possibilities. The intriguing formation of three new C–C bonds that support novel dichromium, dicobalt, and dinickel bonds in **C** is also complicated, and while likely to be derived from azaallyls generated upon deprotonation of the chelate precursor, both radical and 2e⁻ paths to the new C–C bonds are conceivable.⁴

The nature of the C–C bond-forming processes in **C**, in which six stereocenters are set,⁴ showed substantial promise toward constructing ring systems via either mechanistic, radical or nucleophile/electrophile coupling. The connectivity engen-

Received: January 17, 2014

Published: April 24, 2014



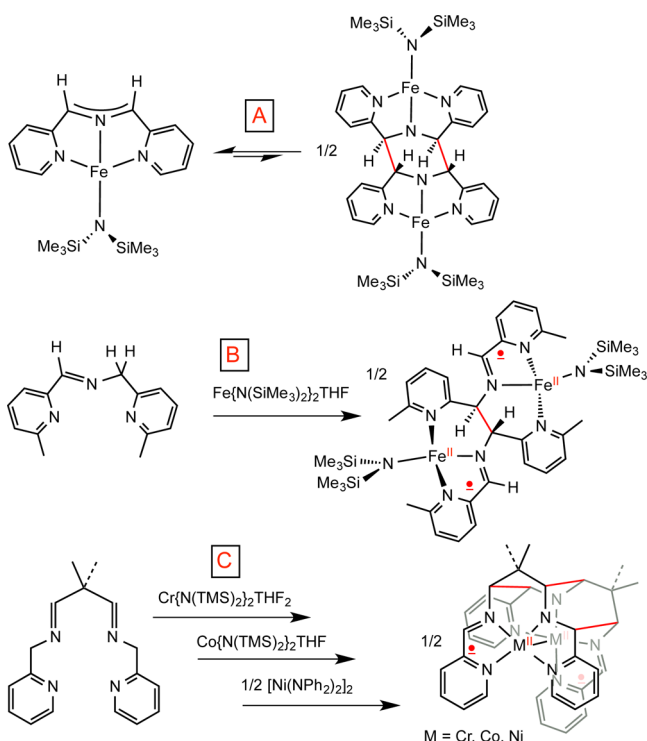


Figure 1. Examples of C–C bond formation (red) derived from the reactivity of azaallyl precursors.

dered by transient azaallyls in combination with pyridine provides a reservoir for electrons via redox noninnocence (RNI).^{7–14} This capability is suspected of aiding in C–C bond formation by enabling the generation of stable metal(II) centers; otherwise, the cobalt, nickel, and chromium derivatives are formally metal(I). Cases in which more than one metal are involved can be rationalized as reductive couplings, and the formation of metal–metal-bonded complexes in C are prime examples.

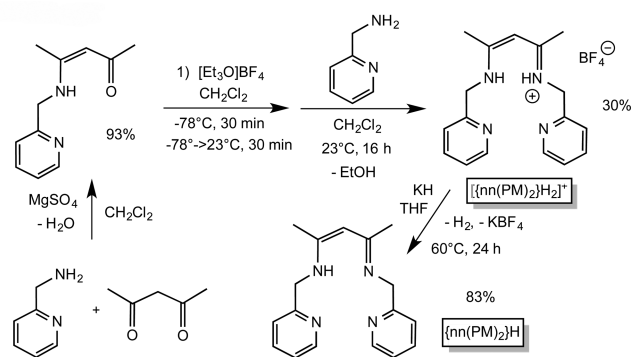
Because an example of a nacnac ligand coupling at the mid-carbon of its backbone was known,¹⁵ related systems in which the connectivity of an azaallyl group was embedded in a nacnac framework^{15–35,37–51} were sought in order to seek out similar reactivity. While no C–C coupling was achieved, insights into RNI were obtained from the ensuing study on iron complexes, and these are presented.

2. RESULTS

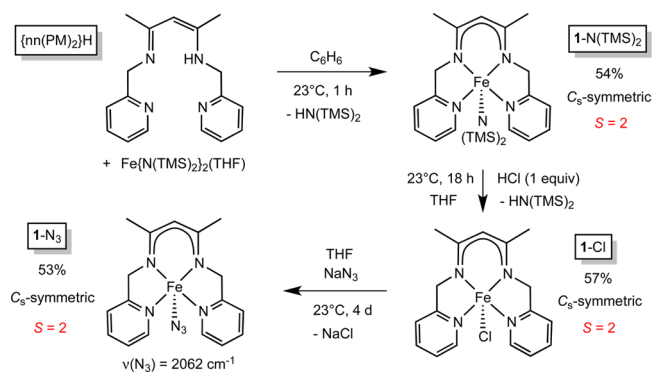
2.1. Ligand Synthesis. A nacnac-based tetradentate chelate^{50,51} was synthesized via the condensation of 2,4-pentanedione with 2-(aminomethyl)pyridine, followed by a second condensation with 2-(aminomethyl)pyridine that required the use of $[\text{Et}_3\text{O}]\text{BF}_4$. The direct product is the protonated $[\{\text{nacnac}-(\text{CH}_2\text{Py})_2\}_2\text{H}_2^+]\text{BF}_4^-$ ($[\{\text{nn}(\text{PM})_2\}_2\text{H}_2]^+$), formed in ~30% yield, as illustrated in Scheme 1. The protonated nacnac is converted to the neutral tetradentate chelate ligand $\{\text{nn}(\text{PM})_2\}_2\text{H}$ in 83% upon treatment with KH in tetrahydrofuran (THF).

2.2. $\{\text{nn}(\text{PM})_2\}_2\text{FeX}$ Compounds. **2.2.1. Synthesis.** As Scheme 2 illustrates, treatment of $\{\text{nn}(\text{PM})_2\}_2\text{H}$ with $\text{Fe}\{\text{N}(\text{TMS})_2\}_2(\text{THF})$ ⁵² in benzene produced 1 equiv of $\text{HN}(\text{TMS})_2$ and orange-red $\{\text{nn}(\text{PM})_2\}_2\text{FeN}(\text{TMS})_2$ [**1-N(TMS)₂**] in 54% yield upon crystallization from pentane. The compound exhibited ¹H NMR spectroscopic shifts (Table 1) indicative of

Scheme 1



Scheme 2



a C_2 -symmetric paramagnetic molecule, consistent with a pseudo-square-pyramidal structure. Measurement of the magnetic susceptibility at 23 °C by the Evans method⁵³ afforded a value of $\mu_{\text{eff}} = 5.3 \mu_{\text{B}}$, indicative of an $S = 2$ center with a significant contribution from spin–orbit coupling (SOC).^{54,55}

The amide group could be cleaved from the iron with 1 equiv of HCl to afford $\text{HN}(\text{TMS})_2$, and the accompanying yellow precipitate, presumably $\{\text{nn}(\text{PM})_2\}_2\text{FeCl}$ (**1-Cl**), was sparingly soluble in common solvents yet could be crystallized from THF/pentane. An Evans method⁵³ measurement conducted in THF at 23 °C afforded $\mu_{\text{eff}} = 5.3 \mu_{\text{B}}$, again indicating an $S = 2$ center with contributions from SOC.^{54,55} The paramagnetic material was assayed by Mössbauer (MB) spectroscopy (vide infra) and by this criteria appeared cleanly prepared. Further attempts to derivatize chloride were severely limited by solubility issues, although treatment of **1-Cl** with NaN_3 for 4 days in THF afforded a similar orange-yellow material that manifested a $\nu(\text{N}_3)$ absorption in its IR spectrum of 2062 cm^{-1} , consistent with substitution of the chloride by azide to form **1-N₃**. Thermal and photochemical conversions of the azide to a nitride were attempted, but thus far no soluble pure material has been isolated.

2.2.2. MB Analysis. Illustrated in Figure 2 are zero-field MB spectra taken on **1-N(TMS)₂** and **1-Cl**. The spectra reflect similar electronic characteristics of the compounds because the respective isomer shifts of 0.96(1) and 0.99(1) mm/s for **1-N(TMS)₂** and **1-Cl** are nearly identical. The values are appropriate for high-spin ferrous centers,^{56–58} thereby corroborating the solution magnetic measurements. The quadrupole splittings of 2.84(1) mm/s for **1-N(TMS)₂** and 3.42(1) mm/s for **1-Cl** are quite large and indicative of substantial asymmetry in the electric field about the

Table 1. ^1H [δ , Coupling (mult, J) or Line Width (*ital.*, $\nu_{1/2}$) in Hz], ^{13}C [δ] and ^{31}P [δ] NMR Data on Coordination Compounds $\{\text{nn}(\text{PM})\}_2\text{FeX}$ (1-X ; $\text{X} = \text{N}(\text{TMS})_2$, Cl , N_3), $[\{\text{nn}(\text{PM})(\text{PI})\}\text{FeLL}]^m$ ($2\text{-LL}'$), and $\{\text{nn}(\text{PM})(\text{PI})\}\text{FeL}$ (3-L)

compd	1/17	2/16	3/15	4/14	5/13	6,6'	7	8	9	10	11	12	18/19	18(^{31}P)
$1\text{-N}(\text{TMS})_2^{a,b}$	96.2 (1380)	38.3 8 (125)	49.17 (110)	-2.45 (70)		10.75 ^c (380)		0.42 (200)	-80.10 (450)				10.75 ^c (380)	
$1\text{-Cl}^{a,d}$	146.27 (770)	38.26 (80)	51.87 (95)	-0.05 (34)		1.57 (30)		5.10 (120)	-84.28 (270)					
$1\text{-N}_3^{a,d}$	156.09 (675)	53.4 5 (100)	133.05 (945)	40.07 (105)		1.29 (20)		5.93 (95)	-82.18 (278)					
$2\text{-}(\text{PMe}_3)_2^b$	8.80 (d, 6)	6.17 (t, 6)	6.61 (t, 6)	6.39 (d, 8)		4.14		2.28	4.99		2.09	6.47	0.66 (d, 6)	19.6 (60)
$2\text{-}(\text{PMe}_2\text{Ph})_2^{b,e}$	7.51 (d, 6)	5.77 (t, 6)	6.60 (t, 7)	6.53 (d, 7)		3.54		2.11	5.47		2.46	6.93	0.85	16.6 (130)
$2\text{-}(\text{PMe}_3)\text{CO}^b$	8.52 (d, 6)	6.12 (t, 6)	6.09 (t, 6)	6.48 (d, 8)		4.68 (br s, 25)		2.08	4.98		2.13	6.41	0.83 (d, 10)	41.2 (880)
$2^{2+}\text{-}(\text{PMe}_3)_2^{d,f}$	7.59 (d, 6)	5.91 (t, 6)	6.68 (t, 6)	6.81 (d, 8)		5.21		2.39	6.47		2.40	8.95	0.93 (dd, 4, 5)	13.8 (10)
$\{\text{nn}(\text{PM})(\text{PI})\}\text{Li}_2^{d'}$	8.01 (d, 7)	6.15 (t, 7)	6.52 (t, 7)	6.55 (d, 7)		4.78		1.62	4.05		1.91	5.37		
3-PMe_3^d	7.79 (d, 6)	5.54 (t, 7)	6.13 (t, 7)	6.24 (d, 7)		4.48		2.48	5.82		2.45	7.24	0.24 (d, 8)	45.0 (220)
$3\text{-PMePh}_2^{b,g}$	8.71 (d, 6)	7.63 (t, 6)	8.10 (t, 7)	7.93 (d, 7)		3.20		2.27	6.45		2.70	8.03	0.38	68.8 (650)
$3\text{-PPH}_3^{b,h}$	8.67 (d, 6)	7.82 (t, 6)	8.12 (t, 7)	7.68 (d, 7)		3.96		2.29	6.23		2.35	7.20		30.5 (1600)
3-CO^d	8.47 (d, 6)	7.16 (t, 7)	7.64 (t, 8)	7.22 (d, 7)		3.60 (d, 21)		2.11	6.31		2.64	7.73		
$2\text{-}(\text{PMe}_3)_2^b$	6.46 (d, 6)	4.61 (t, 7)	5.86 (t, 7)	5.50 (d, 8)		4.21 (d, 21)		2.11	6.31		2.64	7.73		
$2\text{-}(\text{PMe}_2\text{Ph})_2^{b,i}$	9.35 (d, 6)	7.13 (t, 6)	7.42 (t, 7)	7.43 (d, 8)		62.70	149.43	22.26	96.28	136.56	22.10	108.78	13.33	
$2\text{-}(\text{PMe}_3)\text{CO}^b$	7.89 (d, 6)	5.74 (t, 6)	6.34 (t, 7)	6.71 (d, 8)		169.92	149.43	22.26	96.28	136.56	22.10	108.78	13.33	
$2^{2+}\text{-}(\text{PMe}_3)_2^{d,j}$	9.26 (d, 6)	6.17 (t, 6)	6.58 (t, 6)	6.90 (d, 8)		153.90	149.55	22.57	99.34	137.33	22.70	110.93	11.86	
$\{\text{nn}(\text{PM})(\text{PI})\}\text{Li}_2^{d'}$	8.46 (d, 6)	6.59 (t, 6)	6.91 (t, 6)	7.45 (d, 6)		169.48	149.55	22.57	99.34	137.33	22.70	110.93	11.86	
3-PMe_3^d	9.47 (d, 7)	6.82 (t, 7)	6.83 (t, 7)	7.41 (d, 8)		154.07	153.29	22.42	100.42	139.58	22.31	124.42	14.65	
$3\text{-PMePh}_2^{b,g}$	8.78 (d, 7)	6.07 (t, 7)	6.63 (t, 7)	6.97 (d, 7)		174.38	153.29	22.42	100.42	139.58	22.31	124.42	14.65	
3-CO^d	8.95 (d, 6)	6.28 (t, 6)	6.90 (t, 6)	7.34 (d, 7)		152.73	159.45	26.39	128.28	140.77	21.36	135.75	10.84	
$2\text{-}(\text{PMe}_3)_2^b$	8.43 (d, 6)	6.34 (t, 6)	6.65 (t, 6)	6.36 (d, 6)		176.75	159.45	26.39	128.28	140.77	21.36	135.75	10.84	
$2\text{-}(\text{PMe}_3)_2^{d,j}$	155.41	120.83	129.41	117.81		163.53	158.13	19.05	95.48	142.46	22.93	99.24		
$2\text{-}(\text{PMe}_2\text{Ph})_2^{b,i}$	150.61	100.87	125.06	112.80		166.29	158.13	19.05	95.48	142.46	22.93	99.24		
$2\text{-}(\text{PMe}_3)\text{CO}^b$	155.42	117.46	120.75	129.52		153.32	158.13	19.05	95.48	142.46	22.93	99.24		
$2^{2+}\text{-}(\text{PMe}_3)_2^{d,j}$	151.59	101.99	124.98	113.86		170.90	149.36	22.48	103.48	137.37	21.77	112.13	11.99	
$\{\text{nn}(\text{PM})(\text{PI})\}\text{Li}_2^{d'}$	150.25	121.87	134.88	130.43		154.22	149.36	22.48	103.48	137.37	21.77	112.13	11.99	
3-PMe_3^d	138.73	102.03	121.92	118.00		169.63	151.96	21.43	106.93	131.55	22.00	116.44	21.57	
$\{\text{nn}(\text{PM})(\text{PI})\}\text{Li}_2^{d'}$	159.34	128.63	141.92	129.97		155.08	151.96	21.43	106.93	131.55	22.00	116.44	21.57	
3-PMe_3^d	156.14	98.94	142.50	144.35										
$\{\text{nn}(\text{PM})(\text{PI})\}\text{Li}_2^{d'}$	149.63	121.73	137.15	122.60										
3-PMe_3^d	150.63	97.90	130.86	115.62										
$\{\text{nn}(\text{PM})(\text{PI})\}\text{Li}_2^{d'}$	157.67	121.69	130.04	117.93										
$3\text{-PMePh}_2^{b,k}$	151.41	102.91	123.14	114.59										
$3\text{-PMePh}_2^{b,k}$	156.90	120.52	128.38	123.40										
$3\text{-PMePh}_2^{b,k}$	151.28	105.96	123.45	116.10										

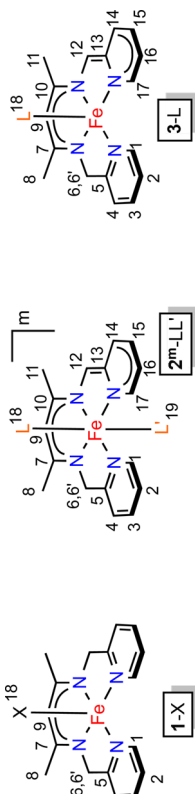


Table 1. continued

compd	1/17	2/16	3/15	4/14	5/13	6,6'	7	8	9	10	11	12	18/19	18(31P)
3-PPh ₃ ^{b,1}	158.21	121.27	125.25	128.51	154.78	67.96	147.64	24.41	108.61	137.69	23.05	128.24		
3-CO ^d	155.80	100.76	120.54	121.76	147.68									
	148.28	106.10	125.42	118.68	166.81	64.88	152.62	21.71	109.11	143.30	21.83	117.33		

^a Assignments tentative. ^b C₆D₆, 400 MHz. ^c Resonances overlap and integrate to ~22 H. ^d THF-*d*₈, 400 MHz. ^e 6.89 (m, P(CH₃)₂Ph, 8 H), 7.00 (m, P(CH₃)₂Ph, 2 H), ^f 7.58 (s, B(3,5-(CF₃)₂-C₆H₃)₄, 8 H), 7.79 (s, B(3,5-(CF₃)₂-C₆H₃)₄, 16 H), ^g 6.71 (m, P(CH₃)Ph₂, 4 H), 6.93 (m, P(CH₃)Ph₂, 6 H), ^h 7.02 (m, PPh₃, 3 H), 7.28 (m, PPh₃, 2 H), ⁱ 110.93 (P(CH₃)₂Ph), 127.76 (P(CH₃)₂Ph), 130.13 (P(CH₃)₂Ph), ^j 119.50 (B(2,5-CF₃(C₆H₃))₄), 136.69 (B(2,5-CF₃(C₆H₃))₄), ^k 127.71 (P(CH₃)Ph₂), 130.85 (P(CH₃)Ph₂), 131.57 (P(CH₃)Ph₂), ^l 128.43 (PPh₃), 128.81 (PPh₃), 134.24 (PPh₃).

nucleus.^{56–58} The N₂N'N''Fe coordination about 1-N(TMS)₂ is likely to be somewhat more symmetric than the set of ligands that provide a N₂N'N''ClFe core, simply because of the greater difference between chloride and amide compared to the chelate nitrogen donors. The five-coordinate, pseudo-square-pyramidal geometries accorded the amide and chloride, and the open nature of the nn(PM)₂ tetradentate chelate should induce substantial asymmetry at the core of the complexes.

2.2.3. {nacnac(PM)₂}FeN(SiMe₃)₂ (1-N(TMS)₂) Structure. Although the MB results support the pseudo-square-pyramidal structures proposed for 1-N(TMS)₂ and 1-Cl, the severe asymmetry reflected in the spectra could be due to solid-state structures in which the chelate is not planar and not averaged as in solution. A single-crystal X-ray structure determination of 1-N(TMS)₂ was conducted, selected data collection and refinement parameters are listed in Table 2, pertinent interatomic distances and angles are given in Table 3, and molecular views of the molecule are given in Figure 3. The actual geometry is difficult to categorize because both highly distorted square-planar and trigonal-bipyramidal descriptions are reasonable.

The logical apical site of a square pyramid is that of the amide, but the angles from its nitrogen to the pyridine, two nacnac, and remaining pyridine nitrogens are 117.6(10)° ave, 112.5(27)° ave, 126.1(2)° ave, and 98.2(20)° ave, respectively. It might be tempting to view one nacnac nitrogen and one pyridine nitrogen as axial constituents of a trigonal bipyramid, but that angle is far from 180° at 149.3(8)° ave, although the N_{py}-Fe-N_{nn} [116.1(10)° ave], N_{nn}-Fe-N_{am} [126.1(2)° ave], and N_{am}-Fe-N_{py} [117.6(10)° ave] angles sum to 359.8°. Bite angles affiliated with the N_{nn}-N_{py} groups are 75.8(13)° ave, and those of the nacnac entity are 84.5(3)° ave. Using the Addison criteria,⁵⁹ τ of 0.58 is found, rendering the molecule essentially between that of a trigonal-bipyramidal structure and one construed as square-pyramidal.

The core distances are normal for high-spin iron(II),²⁶ with long bonds to the pyridines [2.234(7) Å ave and 2.197(5) Å ave], followed by those to the nacnac at 2.087(12) Å ave and 2.104(5) Å ave. The shortest Fe-N bond is to the amide at 2.016(7) Å ave, and the remaining bond distances in the nacnac body of the chelate and those pertaining to the 2-pyridylmethyl arms of the chelate are normal.

2.3. {nn(PM)(PI)}FeL_n Compounds. 2.3.1. Syntheses. The remaining amide on 1-N(TMS)₂ was considered a plausible internal base, and the compound was treated with donors with the hope of affecting dehydroamination, which can be viewed as a deprotonation or reductive elimination, as Figure 4 illustrates. With an excess of PMe₃ (~5 equiv), free HN(TMS)₂ was observed after 24 h at 23 °C in C₆D₆, and the color of the reaction became deeper red as resonances consistent with a new diamagnetic species with C_s symmetry appeared in the ¹H NMR spectrum. Upon scale-up, 2-(PMe₃)₂ was isolated as dark-purple crystals in 71% yield. ¹H NMR spectra indicated that ligand desymmetrization had occurred, causing one arm of the chelate to become unsaturated, as shown in Scheme 3. In the presence of CO, 2-(PMe₃)₂ was rapidly converted to magenta {nn(PM)(PI)}Fe(PMe₃)CO [2-(PMe₃)CO; ν(CO) = 1912 cm⁻¹] at 23 °C in C₆D₆, and its ¹H NMR spectrum was similar to that of its predecessor.

As the carbonyl reaction indicated, one phosphine of 2-(PMe₃)₂ was labile because its repeated exposure to vacuum while in C₆D₆ caused the appearance of a new set of resonances consistent with a diamagnetic complex containing a single

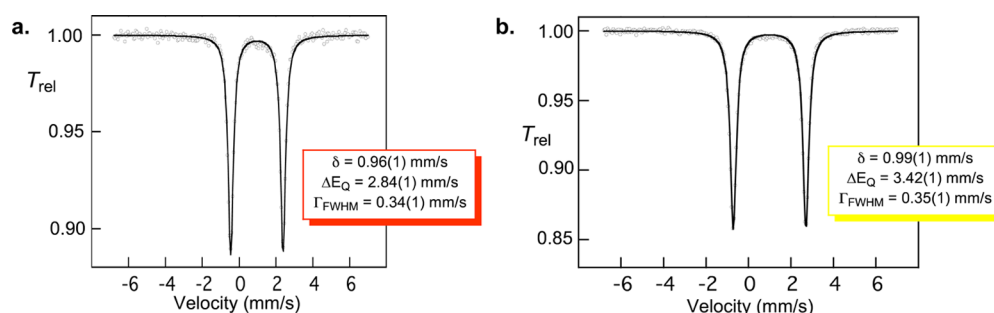


Figure 2. Zero-field MB spectra of 1-N(TMS)₂ (a) and 1-Cl (b) taken at 80 K.

Table 2. Select Crystallographic and Refinement Data for 1-N(TMS)₂, 2-(PMe₃)₂, 3-PMePh₂, and 2⁺-(PMe₃)₂

	1-N(TMS) ₂	2-(PMe ₃) ₂	3-(PMePh ₂)	2 ⁺ -(PMe ₃) ₂
formula	C ₂₃ H ₃₇ N ₃ Si ₂ Fe	C ₂₃ H ₃₆ N ₄ P ₂ Fe	C ₃₀ H ₃₁ N ₄ PFe	C ₂₃ H ₃₆ N ₄ F ₆ P ₃ Fe
formula wt	495.61	486.35	534.41	631.32
space group	P2 ₁ /n	P2 ₁ /c	C2	P2 ₁ 2 ₁ 2
Z	8	4	4	8
a, Å	22.344(4)	10.1579(8)	17.4724(6)	17.6532(14)
b, Å	9.5554(14)	16.4764(12)	10.0996(3)	35.819(3)
c, Å	25.374(4)	15.0780(11)	14.5690(5)	8.8940(7)
α, deg	90	90	90	90
β, deg	98.763(5)	103.175(3)	101.8790(10)	90
γ, deg	90	90	90	90
V, Å ³	5354.4(15)	2457.1(3)	2515.85(14)	5623.9(8)
ρ _{calc} , g/cm ³	1.230	1.315	1.411	1.491
μ, mm ⁻¹	0.672	0.761	0.690	0.767
temp, K	173(2)	173(2)	193(2)	183(2)
λ, Å	0.71073	0.71073	0.71073	0.71073
R indices [I > 2σ(I)] ^{a,b}	R1 = 0.0355, wR2 = 0.0840	R1 = 0.0266, wR2 = 0.0685	R1 = 0.0233, wR2 = 0.0580	R1 = 0.0437, wR2 = 0.0956
R indices (all data) ^{a,b}	R1 = 0.0573, wR2 = 0.0937	R1 = 0.0324, wR2 = 0.0719	R1 = 0.0256, wR2 = 0.0591	R1 = 0.0613, wR2 = 0.1039
GOF ^c	1.026	1.023	1.006	1.012

^aR1 = $\sum ||F_o| - |F_c|| / \sum |F_o|$. ^bwR2 = $[\sum w(|F_o| - |F_c|)^2 / \sum wF_o^2]^{1/2}$. ^cGOF (all data) = $[\sum w(|F_o| - |F_c|)^2 / (n - p)]^{1/2}$, where n = number of independent reflections and p = number of parameters.

PMe₃. While 3-PMe₃ was never generated completely free of 2-(PMe₃)₂, it could be routinely prepared as a brown solid in >90–95% purity via careful removal of PMe₃ upon repeated exposure to vacuum. An alternative preparation via the addition of 1 equiv of PMe₃ to 1-N(TMS)₂ also led to a material of similar purity.

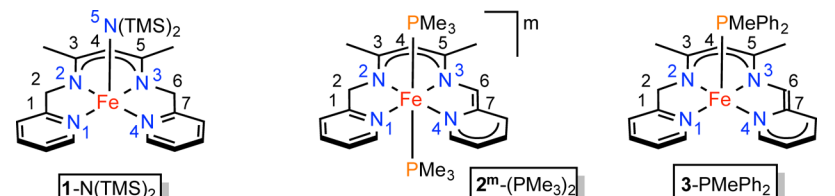
In order to test whether strong σ donors were needed to initiate the internal deprotonation or dehydroamination event, 1-N(TMS)₂ was treated with CO (1 atm) at 23 °C in C₆D₆ and the loss of HN(TMS)₂ was noted over 18 h. Amine generation was accompanied by a new diamagnetic complex whose ¹H NMR spectrum was similar to that of 3-PMe₃. On the basis of the observation of diastereotopic methylene hydrogens and an IR spectrum that revealed a single ν (CO) of 1879 cm⁻¹, the complex, which was isolated as red crystals in 79% yield from pentane, was formulated as {nn(PM)(PI)}FeCO (3-CO).

A synthetic variation was used to explore the tendency of various phosphines to adopt the five-coordinate {nn(PM)(PI)}FePR₂R' or six-coordinate {nn(PM)(PI)}Fe(PR₂R')₂ structures. The nacnac precursor {nn(PM)₂H} was doubly deprotonated with ⁿBuLi to afford the dianion {nn(PM)(PI)}²⁻Li₂, which was treated with FeBr₂(THF)₂ in the presence of excess phosphine to yield brown to purple-brown materials, as shown in Scheme 4. The stronger donors PMe₃ and PMe₂Ph adopted the diphosphine structure, {nn(PM)(PI)}Fe(PR₂R')₂ [2-(PR₂R')₂; PR₂R' = PMe₃, PMe₂Ph], while

the better π acceptors favored formation of the monophosphine derivative, {nn(PM)(PI)}Fe(PR₂R') [3- PR₂R'; PR₂R' = PMePh₂, PPh₃]. The reactions were initially conducted on NMR tube scales, but 3-PMe₂Ph was scaled up for assessment by single-crystal X-ray studies.

In order to probe the redox capability of the {nn(PM)(PI)} ligand, the bis-PMe₃ complex {nn(PM)(PI)}Fe(PMe₃)₂ [2-(PMe₃)₂] was oxidized with ferricinium to afford the brown, crystalline monocation [{nn(PM)(PI)}Fe(PMe₃)₂]⁺PF₆⁻ [2⁺-(PMe₃)₂] on a small scale, but one that yielded material for single-crystal X-ray diffraction. Generation of the dark-green dication [{nn(PM)(PI)}Fe(PMe₃)₂]²⁺(BAR^F₄)₂ [2²⁺-(PMe₃)₂] was accomplished via the addition of 2 equiv of AgBAR^F₄ [BAR^F₄⁻ = B(3,5-(CF₃)₂C₆H₃)₄⁻]⁶⁰ to 2-(PMe₃)₂.

2.3.2. MB Analyses. Additional data probing the iron oxidation state in the six- and five-coordinate species containing the {nn(PM)(PI)}ⁿ (Fe⁰, $n = 0$; Fe^I, $n = 1$ –; Fe^{II}, $n = 2$ –) ligand was obtained via zero-field MB spectra on 2-(PMe₃)₂, 2-(PMe₃)CO, 3-PMe₃, and 3-CO. The isomer shift of $\delta = 0.32(1)$ mm/s for 2-(PMe₃)₂ is substantially lower than those of the high-spin ferrous derivatives described in Figure 5 and in a region typically observed for low-spin Fe^{II}.^{56–58} In addition, its quadrupole splitting of 0.69(1) mm/s reveals a more symmetric electric field at the nucleus in comparison to the previous five-coordinate species, a probable consequence of six-coordination. Related parameters are observed for 2-(PMe₃)-

Table 3. Selected Interatomic Distances (Å) and Angles (deg) for 1-N(TMS)₂, 2-(PMe₃)₂, 3-PMePh₂, and 2⁺-(PMe₃)₂


	1-N(TMS) ₂	2-(PMe ₃) ₂	3-PMePh ₂	2 ⁺ -(PMe ₃) ₂ ^a
Fe–N1	2.1939(13), 2.2009(12)	1.9749(11)	1.9746(10)	1.994(4), 2.001(4)
Fe–N2	2.0788(12), 2.0958(11)	1.9487(11)	1.8847(11)	1.939(4), 1.938(4)
Fe–N3	2.1025(12), 2.1078(12)	1.9648(11)	1.9197(11)	1.945(4), 1.942(4)
Fe–N4	2.2388(12), 2.2296(12)	1.9913(11)	1.9379(10)	2.012(4), 2.000(4)
Fe–N5	2.0113(13), 2.0213(12)			
Fe–P		2.2629(4), 2.2737(4)	2.1630(3)	2.2713(15), 2.2797(16), 2.2703(15), 2.2806(15)
N1–C1	1.334(2), 1.3366(18)	1.3590(17)	1.3597(16)	1.361(6), 1.357(6)
C1–C2	1.501(2), 1.502(2)	1.4831(19)	1.475(2)	1.458(7), 1.447(7)
C2–N2	1.454(2), 1.4566(17)	1.4346(18)	1.4683(17)	1.400(6), 1.408(7)
N2–C3	1.3268(19), 1.3262(18)	1.3453(17)	1.336(2)	1.331(6), 1.335(6)
C3–C4	1.400(2), 1.401(2)	1.393(2)	1.409(2)	1.389(7), 1.386(7)
C4–C5	1.412(2), 1.404(2)	1.416(2)	1.385(2)	1.397(7), 1.384(7)
C5–N3	1.3093(19), 1.3169(19)	1.3303(17)	1.3591(17)	1.341(6), 1.339(6)
N3–C6	1.4575(19), 1.453(2)	1.3931(17)	1.3705(16)	1.388(6), 1.404(6)
C6–C7	1.503(2), 1.500(2)	1.3810(19)	1.382(2)	1.443(7), 1.447(7)
C7–N4	1.3421(19), 1.3462(18)	1.3972(17)	1.4075(14)	1.361(6), 1.365(6)
N5/P–Fe–N1	99.57(5), 96.81(5)	93.18(3), 87.39(3)	90.35(3)	91.32(12), 88.33(12), 92.47(12), 87.05(12)
N5/P–Fe–N2	126.23(5), 126.02(5)	89.85(4), 91.04(4)	103.00(3)	87.40(13), 90.37(13), 87.73(12), 90.71(12)
N5/P–Fe–N3	110.53(5), 114.40(5)	92.26(3), 87.22(3)	93.32(3)	91.17(12), 89.05(12), 90.94(12), 89.44(12)
N5/P–Fe–N4	118.34(5), 116.93(5)	86.45(3), 92.64(3)	103.39(3)	86.15(11), 96.08(12), 87.03(12), 94.54(12)
P–Fe–P	179.00(2)			177.77(6), 178.42(6)
N1–Fe–N2	77.15(5), 76.60(4)	82.81(4)	83.77(5)	82.78(17), 82.48(16)
N1–Fe–N3	149.89(5), 148.79(5)	173.45(4)	175.72(4)	175.53(17), 174.75(17)
N1–Fe–N4	91.63(5), 92.12(5)	100.91(4)	98.94(4)	102.19(17), 101.91(17)
N2–Fe–N3	84.63(5), 84.27(5)	93.58(4)	93.26(5)	93.62(17), 93.67(17)
N2–Fe–N4	115.40(5), 116.81(5)	174.88(5)	153.45(4)	171.93(16), 173.30(16)
N3–Fe–N4	74.70(5), 74.68(5)	83.05(4)	82.35(5)	81.69(16), 82.24(16)
N1–C1–C2	117.48(14), 117.43(12)	115.54(12)	115.73(10)	115.4(4), 116.1(5)
C1–C2–N2	111.68(13), 111.79(11)	111.28(11)	109.96(10)	113.5(5), 113.1(5)
C2–N2–C3	116.96(13), 117.06(11)	118.71(11)	116.51(11)	118.6(4), 118.6(4)
N2–C3–C4	123.76(13), 123.74(13)	122.65(12)	120.94(12)	122.8(5), 121.8(5)
C3–C4–C5	126.45(14), 126.32(14)	128.44(12)	127.78(14)	128.4(5), 130.1(5)
C4–C5–N3	121.49(14), 121.83(13)	122.62(12)	121.87(12)	122.6(4), 121.7(5)
C5–N3–C6	119.98(13), 118.56(13)	121.69(11)	121.06(11)	119.4(4), 119.2(4)
N3–C6–C7	109.45(12), 109.70(12)	116.57(12)	115.06(10)	113.1(4), 112.9(5)
C6–C7–N4	116.51(13), 117.03(13)	116.21(12)	114.16(10)	115.5(4), 115.8(5)

^aDisorder is evident because an asymmetric {nn(PM)(PI)} ligand appears symmetric: $d(\text{N1–C1}) = 1.359(3)$ Å ave and $d(\text{N4–C7}) = 1.363(2)$ Å ave; $d(\text{C1–C2}) = 1.453(8)$ Å ave and $d(\text{C6–C7}) = 1.445(3)$ Å ave; $d(\text{C2–N2}) = 1.404(6)$ Å ave and $d(\text{N3–C6}) = 1.396(11)$ Å ave; $d(\text{N2–C3}) = 1.333(3)$ Å ave and $d(\text{C5–N3}) = 1.340(2)$; $d(\text{C3–C4}) = 1.388(2)$ Å ave and $d(\text{C4–C5}) = 1.391(9)$ Å ave.

CO, which has a low isomer shift of $\delta = 0.08(1)$ mm/s in a region fairly common for carbonyl derivatives, and ΔE_Q of 0.37(1) mm/s indicative of a fairly symmetric electric field consistent with six-coordination.

The monophosphine and monocarbonyl derivatives, {nn-(PM)(PI)}FeL (L = PMe₃, 3-PMe₃; L = CO, 3-CO), have isomer shifts of δ 0.17 and δ 0.14 mm/s, respectively, which are in a rather nebulous region that can be assigned to several oxidation states but mostly to low-spin species that exhibit significant covalency. The quadrupole splittings of 3-CO and 3-PMe₃ are 1.13 and 1.62 mm/s, respectively, which presumably reflect the electronic asymmetry intrinsic to five-coordination in

a low-spin environment. For reference, isomer shifts of around -0.1 mm/s are observed for Fe(CO)₅ and Fe(CO)₄PPh₃,⁶¹ two complexes with formal Fe⁰ oxidation states but ones in which the carbonyl ligands effectively reduce the electron density at the iron due to their back-bonding properties. Strong-field ferrous compounds, such as low-spin { κ -N,N'-neoPeN=CH(2-pyridyl)}₂FeMe₂ ($\delta = 0.19$, $\Delta E_Q = 1.24$),⁶² are also found in this regime, hence the ambiguity in the assignment of formal oxidation states.⁶³ In contrast to 3-PMe₃, { κ -N,N'-neoHexN=CH(2-pyridyl)}₂FePMe₃,^{62,64} which contains two PI radical anions and is formulated as Fe^{II}, has an isomer shift of δ 0.32 mm/s but a similar ΔE_Q of 1.63 mm/s.

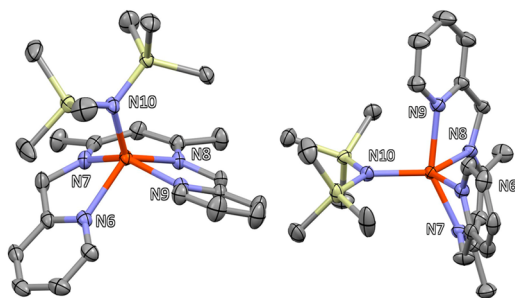


Figure 3. One of two independent 1-N(TMS)_2 molecules in configurations showing the structural ambiguity between square-pyramidal (N10 apical) and trigonal-bipyramidal (N7 and N9 axial) geometries.

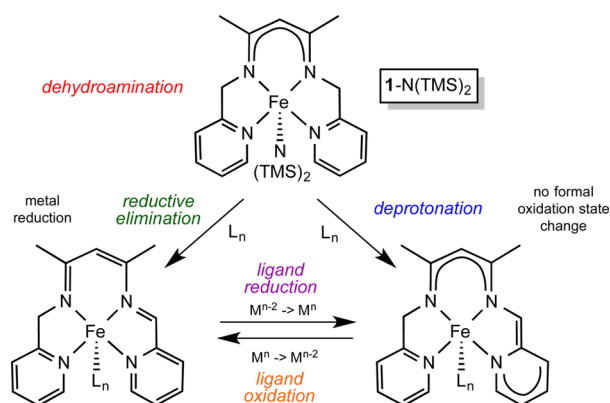
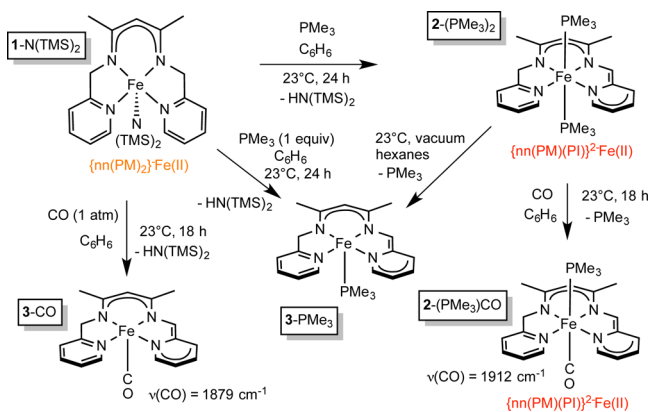


Figure 4. Dehydroamination viewed as either a reductive elimination or deprotonation.

Scheme 3



Perhaps the closest analogy is to $(\text{PDI})\text{Fe}(\text{X}/\text{L})_2$ complexes, whose isomer shifts change from a high-spin range⁶⁵ to around 0.0 for dicarbonyl derivatives.⁶⁶

2.3.3. Electron Paramagnetic Resonance (EPR) Spectrum of $2^+(\text{PMe}_3)_2$. While sample degradation proved somewhat problematic (see the Supporting Information, SI), the rhombic EPR spectrum in Figure 6 is consistent with its assignment to $S = 1/2$ $2^+(\text{PMe}_3)_2$. g_{ave} for the spectrum is 2.058 ($g_1 = 2.014$, $g_2 = 2.036$, and $g_3 = 2.125$), which may be interpreted as a metal-localized singly occupied molecular orbital (SOMO) with substantial ligand character^{67–69} or a ligand radical with substantial metal character; i.e., the electron resides in an orbital of significant covalency. Coupling to two equivalent phosphorus nuclei is observed for g_3 , with $A_3 = 256$ MHz, a

large value even for an orbital with considerable phosphorus character.

2.3.4. $2\text{-(PMe}_3)_2$ Structure. A single-crystal X-ray structure determination of $2\text{-(PMe}_3)_2$ was conducted, and assorted data collection and refinement parameters are given in Table 2. Molecular views are illustrated in Figure 7, and metric parameters may be found in Table 3. The complex is pseudooctahedral, with a slight twist ($\sim 9^\circ$) of the chelate providing a subtle C_2 distortion away from true C_{2v} symmetry. It is difficult to discern the $-\text{CH}=\text{N}-$ side from the $-\text{CH}_2\text{N}=\text{C}$ sides of the chelate based on angles because N1-Fe-N2 and N3-Fe-N4 are $82.81(4)^\circ$ and $83.05(4)^\circ$, respectively. The nacnac portion of the chelate has a $93.58(4)^\circ$ bite angle, and the pyridine nitrogens are somewhat splayed at an angle of $100.91(4)^\circ$. The phosphines reside at $89.6(27)^\circ$ (P1-Fe-N ave) and $90.4(30)^\circ$ (P2-Fe-N ave) with respect to the chelate nitrogens, and their subtle angular variations appear to be in response to the chelate twist. It is the distances that determine the sides of the chelate because $d(\text{N3-C10})$ of $1.393(2)$ Å is considerably shorter than that of N2-C6 [$1.435(2)$ Å]. Moreover, $d(\text{C10-C11})$ of $1.381(2)$ Å is also shorter than that expected for an $\text{C}(\text{sp}^2)\text{-C}(\text{sp}^2)$ single bond (1.46 Å)⁷⁰ and substantially shorter than C5-C6 [$1.483(2)$ Å]. While the nacnac portion of the chelate has roughly symmetrical bonds, another anomaly is revealed in the C-N_{py} distances adjacent to the arms of the chelate. On the deprotonated side, $d(\text{N4-C11})$ is $1.397(2)$ Å, which is elongated in comparison the 2-pyridylmethylene side, where $d(\text{N1-C5})$ is $1.359(2)$ Å. While the difference is small, it is nonetheless indicative of some anionic character introduced into the imine side of the chelate via RNI.^{48,49} The core distances are normal, with the nacnac Fe-N distances of $1.9487(11)$ Å (N2) and $1.9648(11)$ Å (N3) somewhat shorter than those corresponding to the pyridine nitrogens [N1, $1.9749(11)$ Å; N4, $1.9913(11)$ Å]. Note that the Fe-N distances on the deprotonated side are longer than those attributed to the 2-pyridylmethylene arm. Given the subtle changes of the chelate PM and PI arms and the lack of any complementary studies, calculations were employed to substantiate the claim of RNI and to corroborate the structural implications.

2.3.5. Calculation of $2\text{-(PMe}_3)_2$. Figure 8 displays an molecular orbital (MO) diagram of $2\text{-(PMe}_3)_2$ that reveals the redox noninnocent behavior of the $\{\text{nn}(\text{PM})(\text{PI})\}$ ligand. RNI is primarily a consequence of ligand and metal d-orbitals whose roughly similar energies result in MOs that can be decidedly mixed in composition.^{8–14} In the case of typical PIs or the nacnac-derived orbital herein, the M-L interaction is quite weak, and bonding and antibonding combinations exist within a relatively small energy range. Shown in Figure 8 are bonding and antibonding orbitals derived from d_{xz} and a filled ligand π orbital that are roughly 50:50 in composition. Taking account of the percent composition, the lower four filled, d-based orbitals comprise a “ t_{2g} ” set pertaining to a d^6 Fe^{II} metal center. Note that the highest occupied molecular orbital (HOMO) in the system is a π^* -ligand orbital that has undergone reduction by the iron to essentially render $\{\text{nn}(\text{PM})(\text{PI})\}^n$ as a dianion ($n = 2-$). The orbital is well below the energies of the d_z^2 and $d_{x^2-y^2}$ orbitals (the “ e_g ” set) of the pseudooctahedral molecule.

In the chemistry of ligated PIs, metric parameters for the three redox states have been established,^{71,72} and they are shown in Figure 9. Adding a nacnac portion to a PI to generate

Scheme 4

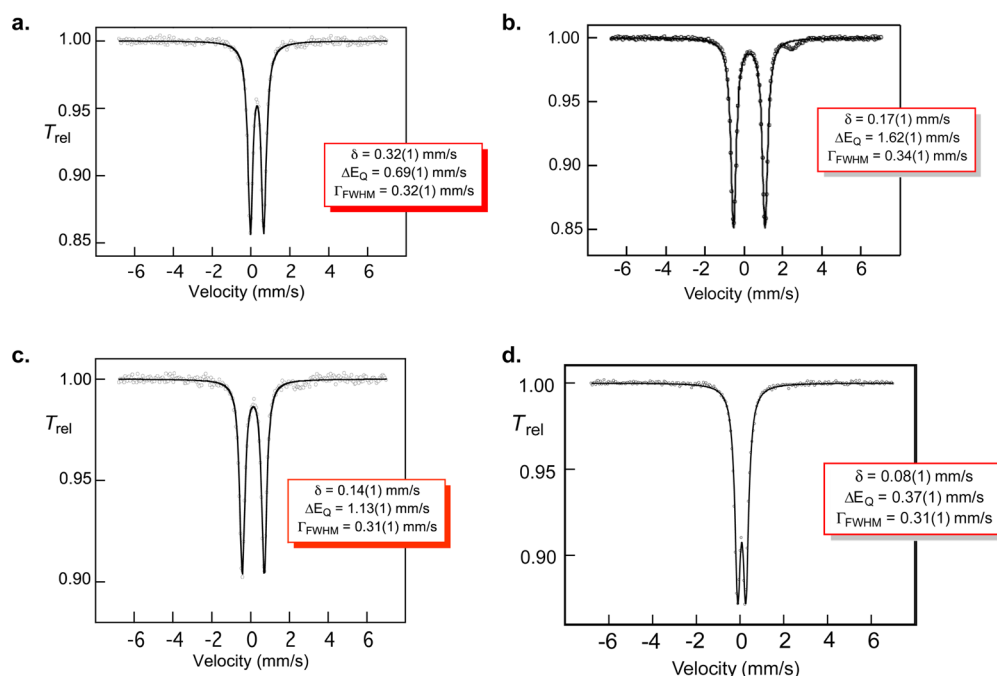
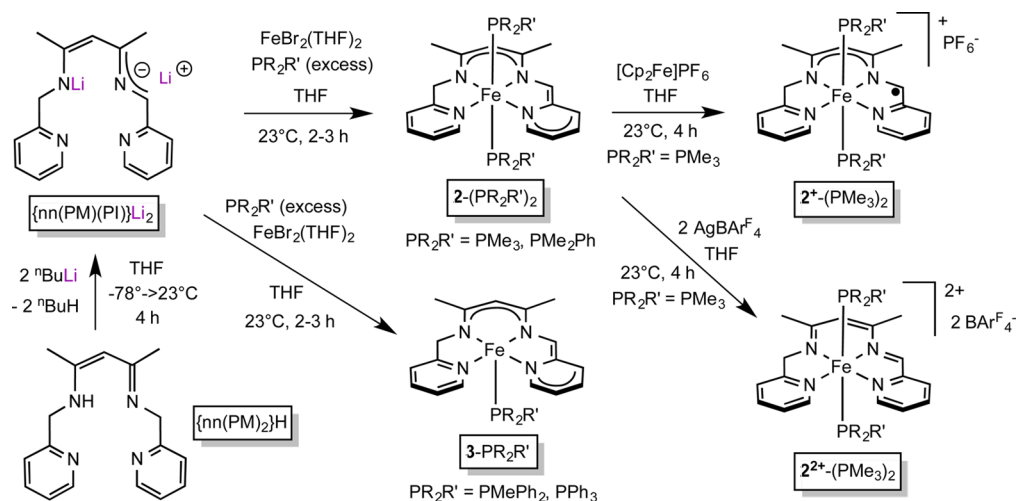


Figure 5. Zero-field MB spectra of $2-(PMe_3)_2$ (a), $3-PMe_3$ (b), $3-CO$ (c), and $2-(PMe_3)CO$ (d) taken at 80 K.

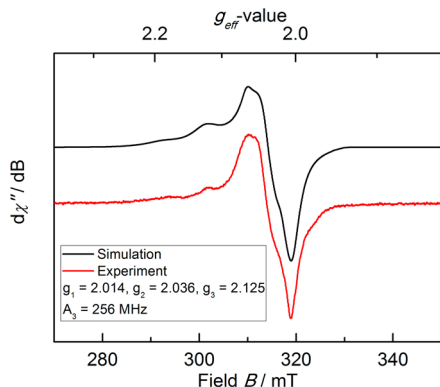


Figure 6. EPR spectrum of $2^+-(PMe_3)_2$ in frozen dimethyl ether (0.5 mM, 8.954 GHz), revealing coupling to two equivalent ^{31}P nuclei ($A_3 = 256$ MHz).

the $\{nn(PM)(PI)\}^n$ ligand changes its nature, and all of the PI parameters do not apply.⁷³ In Figure 8, the chelate is shown to be $\{nn(PM)(PI)\}^{2-}$ in $2-(PMe_3)_2$ based on the orbital occupancies discussed above, but the related $d(N_{nn}=C_{im}) = 1.393(2)$ Å (1.38 Å calc), $d(C_{im}-C_{py}) = 1.381(2)$ Å (1.38 Å calc), and $d(C_{py}-N_{py}) = 1.397(2)$ Å (1.40 Å calc) only partly correspond to a PI ligand because of increased delocalization into the nacnac framework.

2.3.6. $2^+-(PMe_3)_2$ Structure. In order to further examine the various redox states of the $\{nn(PM)(PI)\}^n$ ligand, an X-ray structural study of $2^+-(PMe_3)_2$ was undertaken with mixed results. Table 2 provides selected data collection and refinement details, and the observed metric parameters are listed in Table 3. The two independent molecules found in the asymmetric unit are indistinguishable by eye from the neutral species in Figure 7 and are not illustrated. Unfortunately, disorder renders the bond distances of the methylene and imine sides of $\{nn(PM)(PI)\}^n$ indistinguishable [note that a mixture

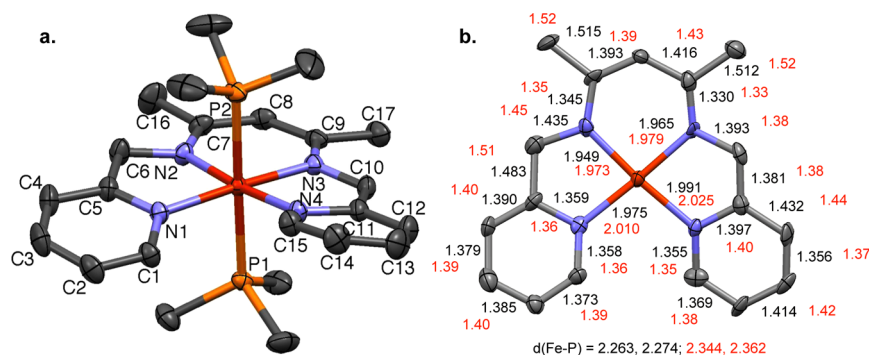


Figure 7. Views of $2-(\text{PMe}_3)_2$ showing the entire molecule (a) and the plane of the chelate (b) as numbered in part a with experimental [black, esd's: Fe–N (0.0011 Å), Fe–P (0.0004 Å), others (0.002–0.003 Å); see Table 3 for full details] and calculated (red) bond distances.

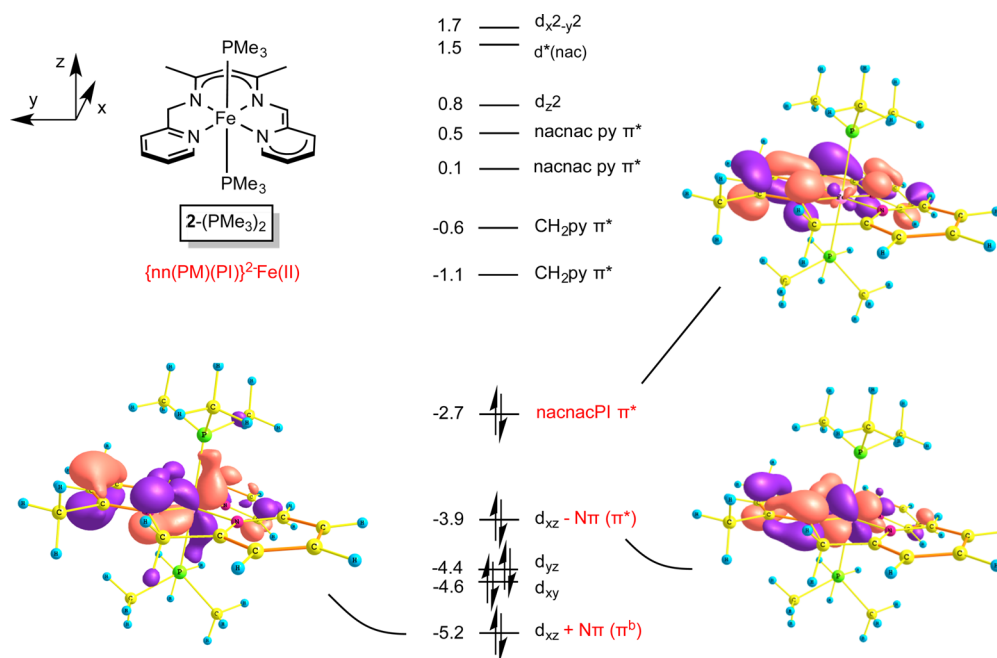


Figure 8. Truncated MO diagram (energies in eV) of $2-(\text{PMe}_3)_2$ showing the ligand π^* -localized HOMO and two MOs (red) of mixed composition: $\sim 50\%$ Fe and $\sim 50\%$ $\{\text{nn}(\text{PM})(\text{PI})\}$. Considering the percent composition of these orbitals, $2-(\text{PMe}_3)_2$ is best construed as $d^6 \text{Fe}^{\text{II}}$.

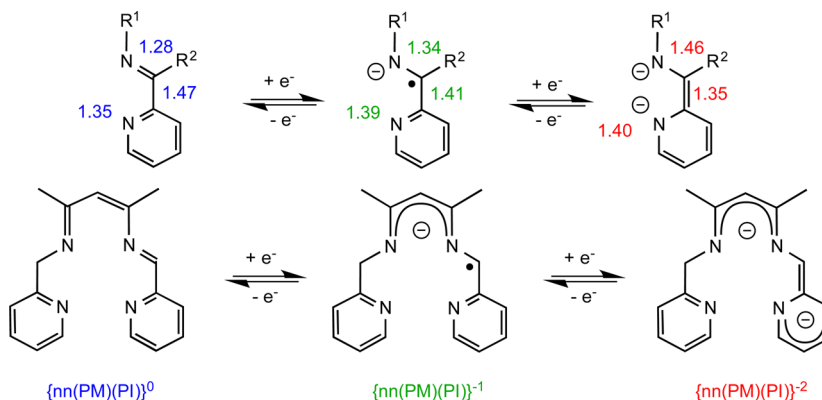


Figure 9. Valence bond structures for the $\{\text{nn}(\text{PM})(\text{PI})\}^n$ ligand showing neutral ($n = 0$, blue), radical anion ($n = 1^-$, green), and dianion ($n = 2^-$, red) redox forms and comparison with PIs similarly classified with $d(\text{N}=\text{C}_{\text{im}})$, $d(\text{C}_{\text{im}}-\text{C}_{\text{py}})$, and $d(\text{C}_{\text{py}}-\text{N}_{\text{py}})$ given in angstroms.

of the neutral complex $2-(\text{PMe}_3)_2$ and dication $2^{2+}-(\text{PMe}_3)_2$ cannot formally be ruled out]. The average distances from Table 3 for $d(\text{N}_{\text{nn}}=\text{C}_{\text{im}})$, $d(\text{C}_{\text{im}}-\text{C}_{\text{py}})$, and $d(\text{C}_{\text{py}}-\text{N}_{\text{py}})$ are 1.400(2), 1.449(6), and 1.361(2) Å, respectively. Assuming that these constitute 1:1 averages of the methylene and imine sides

of the $\{\text{nn}(\text{PM})(\text{PI})\}^n$ ligand and using the corresponding methylene unit distances from the structure of $2-(\text{PMe}_3)_2$, critical π bond distances can be estimated as $d(\text{N}_{\text{nn}}=\text{C}_{\text{im}}) \sim 1.365$ Å, $d(\text{C}_{\text{im}}-\text{C}_{\text{py}}) \sim 1.415$ Å, and $d(\text{C}_{\text{py}}-\text{N}_{\text{py}}) \sim 1.363$ Å. These match calculated values of a monoanionic $\{\text{nn}(\text{PM})-$

(PI)}⁻ ligand, and the remaining distances and angles of 2⁺-(PMe₃)₂ are very close to those of the neutral complex and may be scrutinized in Table 3.

2.3.7. Calculation of 2⁺-(PMe₃)₂. Figure 10 illustrates the framework of the [{nn(PM)(PI)}Fe(PMe₃)₂]^m [*m* = 0, 2-

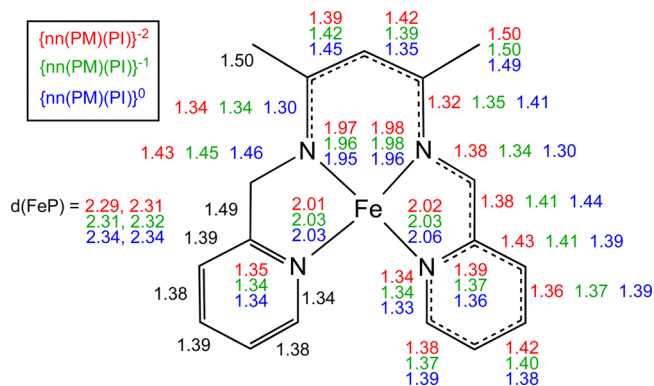


Figure 10. MO6/6-311+G(d)-calculated bond distances for [{nn(PM)(PI)}ⁿFe(PMe₃)₂]^m [*m* = 0, 2-(PMe₃)₂, red; 1+, 2⁺-(PMe₃)₂, green; 2+, 2²⁺-(PMe₃)₂, blue], indicating neutral (*n* = 0, blue), radical anion (*n* = 1-, green), and dianion (*n* = 2-, red) redox forms of the {nn(PM)(PI)}ⁿ ligand.

(PMe₃)₂; 1+, 2⁺-(PMe₃)₂; 2+, 2²⁺-(PMe₃)₂] complexes and calculated bond distances attributed to each chelate linkage. There is a clear demarcation between the redox states of the imine side of the chelate, although they are attenuated from the corresponding bond lengths in the simpler PIs.^{71,72} The values for the monocation are also gratifyingly close to those estimated from the disordered crystal structure, and those of the dication approach those of PI ligands, because delocalization of charge in the neutral ligand is no longer a critical factor. A ready interpretation from the calculated metrics is that Fe^{II} is present in all three derivatives; the redox changes are occurring solely at the ligand.

In Figure 11, partial MO diagrams of [{nn(PM)(PI)}Fe(PMe₃)₂]^m [*m* = 0, 2-(PMe₃)₂; 1+, 2⁺-(PMe₃)₂; 2+, 2²⁺-(PMe₃)₂] are shown, and while the energies of the orbital manifolds are significantly different because of the effects of ionization, the d- and ligand-based orbitals are clearly correlated. The critical orbitals of 2-(PMe₃)₂ illustrated in Figure 8 remain unchanged upon oxidation, and an electron appears to have been removed from {nn(PM)(PI)}²⁻ to afford Fe^{II} chelated by a monoanionic ligand. The proximity of the SOMO to d orbitals of the same symmetry provides mixing that renders its composition mostly ligand-based, but with some iron character, consistent with the EPR spectrum given in Figure 6. The MB spectrum of 2⁺-(PMe₃)₂ was consistent with the calculated model, with $\delta = 0.35(1)$ mm/s and $\Delta E_Q = 0.52(1)$ mm/s [$\Gamma_{\text{fwhm}} = 0.36(1)$ mm/s] indicative of a relatively symmetric ferrous center (see the SI).

2.3.8. 2²⁺-(PMe₃)₂ Calculation. X-ray diffraction experiments on [{nn(PM)(PI)}Fe(PMe₃)₂]²⁺[B(3,5-(CF₃)₂C₆H₃)₄]⁻]₂ [2-(PMe₃)₂]²⁺ failed to elicit a soluble model (see the SI); hence, calculations were relied upon for geometric and electronic details. The calculated distances for the PI side of {nn(PM)(PI)} in 2²⁺-(PMe₃)₂ reflect a neutral ligand because the imine distance of 1.30 Å approaches that of a PI group (1.28 Å), and $d(\text{C}_{\text{im}}-\text{C}_{\text{py}})$ is nearly a typical sp²-sp² C-C single bond at 1.44 Å (Figure 9).⁷⁰ Figure 10 reveals that the second oxidation removes an electron from the ligand-localized HOMO, rendering {nn(PM)(PI)}ⁿ neutral (*n* = 0) and coordinated to Fe^{II}, albeit with roughly the same four fully occupied orbitals, two of which are of mixed d_{zz}/ligand composition. The core distances elongate upon sequential oxidations, despite the iron remaining in the same formal oxidation state for all three compounds. Contraction of the 3d orbitals occurs to a greater extent as the electrostatic perturbation by the ligand diminishes upon undergoing sequential oxidations to the cation and dication.⁷⁴ Metal-ligand overlap and covalency are both attenuated as a consequence, leading to modestly longer $d(\text{Fe}-\text{N})$ and $d(\text{Fe}-\text{P})$. The MB spectrum of 2²⁺-(PMe₃)₂ was consistent with the calculated model, with $\delta = 0.33(1)$ mm/s

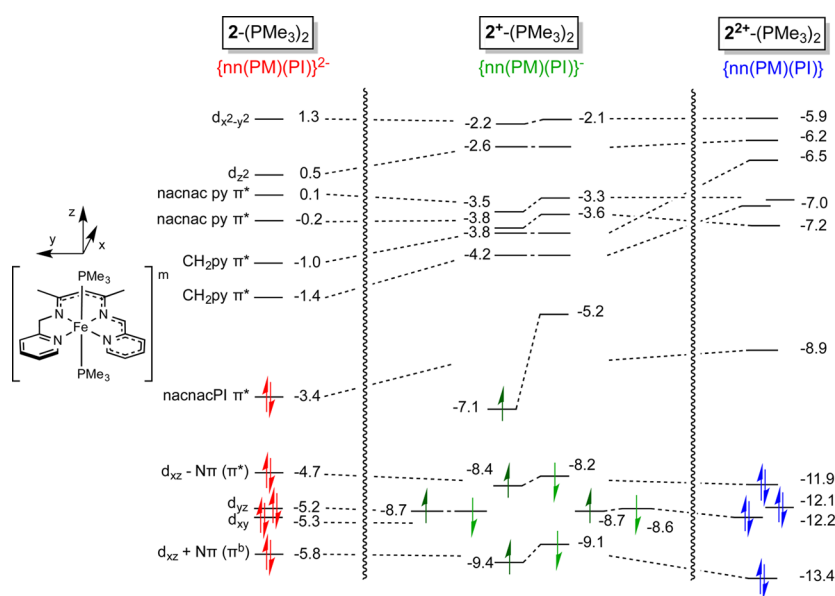


Figure 11. Partial MO diagrams (energies in eV) for [{nn(PM)(PI)}Fe(PMe₃)₂]^m [*m* = 0, 2-(PMe₃)₂, red; 1+, 2⁺-(PMe₃)₂, green; 2+, 2²⁺-(PMe₃)₂, blue]. Note the energy-scale differences for each species that reflect the sequential 1e⁻ ionizations to cation and dication. For 2⁺-(PMe₃)₂, α and β 1e⁻ orbitals reveal the effects of spin polarization.

and $\Delta E_Q = 0.25(1)$ mm/s [$\Gamma_{\text{fwhm}} = 0.24(1)$ mm/s] indicative of a very symmetric low-spin ferrous center (see the SI). In the ^1H NMR spectrum of $2^{2+}\text{-(PMe}_3)_2$, significant downfield shifts are noted relative to $2\text{-(PMe}_3)_2$, especially for hydrogens attached to the central nacnac and imine carbons, consistent with a significant change in the electron density at the ligand, in support of its neutral state.

2.3.9. $\{\text{nn}(\text{PM})(\text{PI})\}\text{Fe}(\text{PMePh}_2)$ (3-PMePh_2) Structure. The five-coordinate derivatives, $\{\text{nn}(\text{PM})(\text{PI})\}\text{FeL}$ ($L = \text{CO}, 3\text{-CO}$; $L = \text{PMe}_3, 3\text{-PMe}_3$; $L = \text{PMePh}_2, 3\text{-PMePh}_2$; $L = \text{PPh}_3, 3\text{-PPh}_3$), are interesting cases in that ^1H NMR spectral shifts of the lone nacnac and imine protons are shifted downfield from the corresponding sites of the six-coordinate species by >1 ppm each. The *o*-hydrogens on one pyridine are also shifted by ~ 1 ppm from the six-coordinate values. Downfield shifts typically indicate changes in the electron density, perhaps brought about by the redox state of the $\{\text{nn}(\text{PM})(\text{PI})\}$ ligand, but are also prone to effects of the coordination environment.

In an effort to understand the changes, an X-ray crystal structure of a representative 3-L species was sought, and 3-PMePh_2 readily provided brown crystals from THF/pentane. Data collection and refinement information can be found in Table 2, while Table 3 lists metric parameters for a comparison with the previous structures. Monophosphine 3-PMePh_2 is roughly square-pyramidal ($\tau = 0.37$)⁵⁹ with (N1–N4)–Fe–P angles of $90.35(3)^\circ$, $103.00(3)^\circ$, $93.32(3)^\circ$, and $103.39(3)^\circ$, respectively, that reflect a twist in the chelate framework, as illustrated in Figure 12. The nacnac bite angle is $93.26(5)^\circ$, and

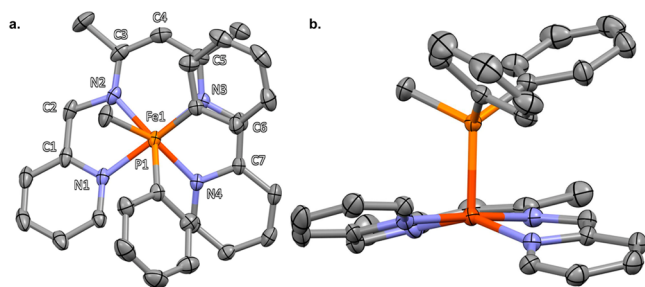


Figure 12. Molecular views of 3-PMePh_2 parallel to the P1–Fe bond (a) and perpendicular to it (b), with the latter showing the twisted nature of the $\{\text{nn}(\text{PM})(\text{PI})\}$ chelate.

the pyridylmethyl bite of $83.77(5)^\circ$ is slightly greater than that of PI [$82.35(5)^\circ$] as expected. The opening (N1–Fe–N4) between the pyridines is $98.94(4)^\circ$, which is partly a consequence of the chelate twist and partly due to the $<90^\circ$ bite angles of the PM and PI arms. The $d[\text{Fe}-(\text{N1}-\text{N4})]$ distances are $1.9746(10)$, $1.8847(11)$, $1.9197(11)$, and $1.9379(10)$ Å, and the latter three are roughly 0.05 Å shorter than the corresponding distances in $2\text{-(PMe}_3)_2$, presumably a testament to the lower coordination number and lesser repulsive interactions about the metal.

The critical bond distances that comprise the imine arm of the ligand are $d(\text{N}_{\text{im}}-\text{C}_{\text{im}}) = 1.371(2)$ Å, $d(\text{C}_{\text{im}}-\text{C}_{\text{py}}) = 1.382(2)$ Å, and $d(\text{C}_{\text{py}}-\text{N}_{\text{py}}) = 1.408(2)$ Å, which are very similar to those of the diphosphine $2\text{-(PMe}_3)_2$. From the bond criteria illustrated in Figure 10, the $\{\text{nn}(\text{PM})(\text{PI})\}^n$ ligand appears to be a dianion, and the complex should be considered as an $\text{Fe}^{\text{II}}, 16e^-$ species.^{64,66} The upfield chemical shifts do not appear to be a consequence of the formal redox state of the $\{\text{nn}(\text{PM})(\text{PI})\}^{2-}$ ligand but perhaps reflect the general decrease

in the electron density upon a change from the six-coordinate, $\text{Fe}^{\text{II}}, 18e^-$ species to the five-coordinate, $\text{Fe}^{\text{II}}, 16e^-$ complex.

2.3.10. $\{\text{nn}(\text{PM})(\text{PI})\}\text{FeL}$ ($L = \text{PMePh}_2, 3\text{-PMePh}_2, \text{CO}, 3\text{-CO}$) Calculations. Calculations of 3-PMePh_2 afforded the truncated MO diagram given in Figure 13, which is quite similar to that of $2\text{-(PMe}_3)_2$. Eight electrons are dispersed into the lowest four orbitals, two that are relatively pure d_{xy} and d_{xz} orbitals and two that are composed of d_{yz} and a ligand. An additional two electrons populate the HOMO that has a modest ($\sim 20\%$) $d_z^2 \sigma^*$ component but is $\sim 80\%$ ligand-based mostly in PI. As a consequence, the compound is best construed as $\text{Fe}^{\text{II}}, d^6$, and $16e^-$. The remainder of d_z^2 is in a high-energy σ^* orbital close to $d_{x^2-y^2}$, which is the main σ^* orbital in relation to the chelate nitrogens, and both are significantly above the HOMO. The HOMO shows an apparently weak $d_z^2/\{\text{PI}(\pi) + \text{nn}(\pi)\}$ overlap that is often treated by broken-symmetry density functional theory,^{75,76} but in this case, a higher-energy solution was obtained by this method.

Recall that 3-CO has a lower CO stretching frequency (1879 cm^{-1}) than the one corresponding to six-coordinate $2\text{-(PMe}_3)_2\text{CO}$ (1912 cm^{-1}). The higher-coordinate ferrous species might be expected to produce the lower CO stretching frequency because of an increase in the electron density. Additional calculations were performed on 3-CO and $2\text{-(PMe}_3)_2\text{CO}$, and the trans influence of PMe_3 is the most probable cause of the higher stretching frequency for the latter. The $\{\text{nn}(\text{PM})(\text{PI})\}$ ligand was calculated to possess roughly the same metrics, but $d(\text{Fe}-\text{C})$ on $2\text{-(PMe}_3)_2\text{CO}$ is 0.08 Å longer [and $d(\text{C}-\text{O})$ is 0.01 shorter] than that of 3-CO . In addition $d(\text{Fe}-\text{N})$ increased by ~ 0.04 Å (ave) for the six-coordinate species, presumably because of an increase in the coordination number. Because the Fe–C distance is longer on $2\text{-(PMe}_3)_2\text{CO}$, the critical overlap for back-bonding is diminished. Figure 14 illustrates the HOMO–1 orbitals for $2\text{-(PMe}_3)_2\text{CO}$ and 3-CO , and greater Fe–C π overlap for the latter is readily seen. The orbital orderings and populations for the carbonyl complexes are similar to those of $2\text{-(PMe}_3)_2$ (Figure 8) and 3-PMePh_2 (Figure 13).

3. DISCUSSION

3.1. RNI of $\{\text{nn}(\text{PM})(\text{PI})\}\text{FeL}_n$. Computational support for $\text{RNI}^{5-15,48,49,64,66,71-73,75-88}$ of the $\{\text{nn}(\text{PM})(\text{PI})\}^n$ ligand parallels the experimental data and provides critical geometric parameters for $n = 0$ and $1-$, for which there is limited structural information. To further substantiate the dianionic character of the $\{\text{nn}(\text{PM})(\text{PI})\}^{2-}$ ligand in $\{\text{nn}(\text{PM})(\text{PI})\}\text{FeLL}'$ ($2\text{-L}, \text{L}'$) and $\{\text{nn}(\text{PM})(\text{PI})\}\text{FeL}$ (3-L) and its likely monoanionic character in $2^+\text{-(PMe}_3)_2$, corresponding hypothetical Mg^{2+} and Li^+ derivatives were calculated at the same MO6/6-311+G(d) level of theory as the iron complexes. Metrics of hypothetical $[\{\text{nn}(\text{PM})(\text{PI})\}]^-\text{Li}$ and $[\{\text{nn}(\text{PM})(\text{PI})\}]^{2-}\text{Mg}$ species corroborate the distances in Figure 10, the experimental ligand dianion distances of $2\text{-(PMe}_3)_2$, and the estimated monoanion ligand bond lengths in $2^+\text{-(PMe}_3)_2$.

A significant ambiguity persists in the monocation because the EPR spectrum in Figure 6 can be interpreted as corresponding to an electron in either a ligand- or metal-based SOMO. Figure 15 illustrates the highest occupied α -orbital electron, i.e., the SOMO (-7.1 eV in Figure 11), and shows that it is clearly ligand-based, with a spin density indicative of approximately 5% iron character. The deviation of g_{ave} from a typical organic radical value of 2.00 can be attributed

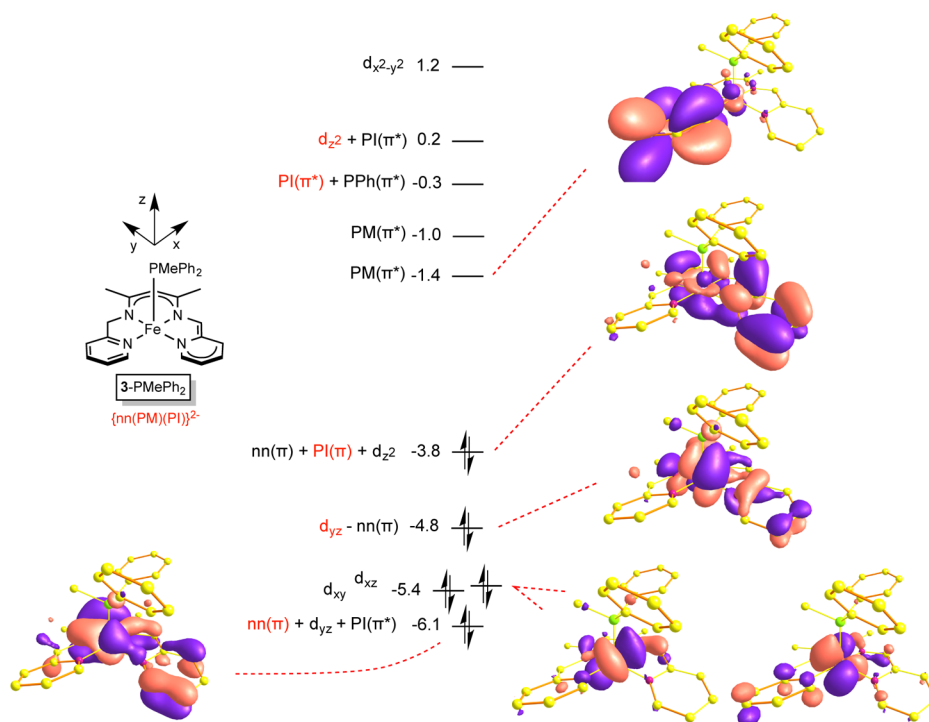


Figure 13. Truncated MO diagram of 3-PMePh₂ showing the frontier orbitals, many with mixed composition. For the latter, the major component is given in red. 3-PMePh₂ is best considered d⁶ Fe^{II}.

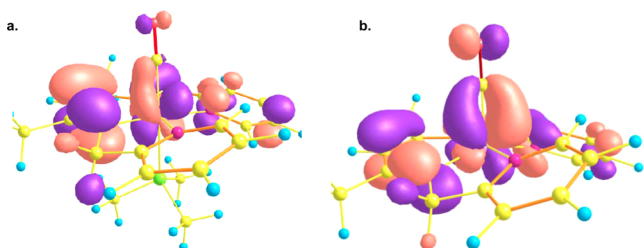


Figure 14. Comparison of the principle π -back-bonding orbitals of 2-(PMe₃)CO [a; $\nu(\text{CO}) = 1912 \text{ cm}^{-1}$] and 3-CO [b; $\nu(\text{CO}) = 1879 \text{ cm}^{-1}$].

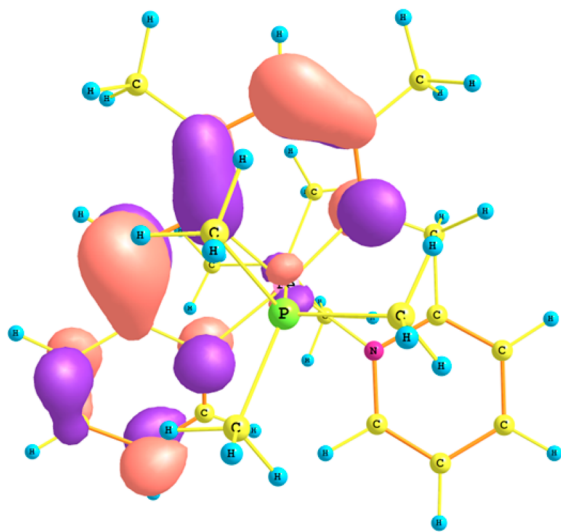


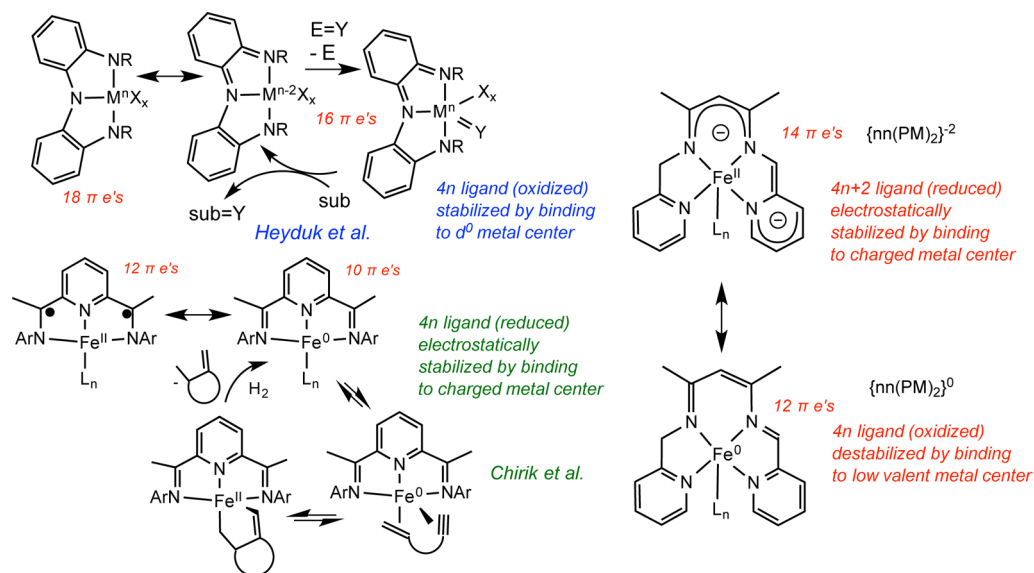
Figure 15. Calculated [M06/6-311+G(d)] highest-energy α -orbital (SOMO) for the optimized doublet geometry corresponding to 2⁺-(PMe₃)₂.

to the modest metal component, provided it is a $d\pi$ type as illustrated, but the large 256 MHz coupling to two equivalent phosphorus nuclei is incommensurate with the π -type orbital illustrated, at least on the basis of a Fermi contact criterion. As a consequence, either the calculations are in error regarding the SOMO composition or the coupling derives from spin polarization, with few other contributions.^{89–91} It is conceivable that an electron in the extended, semicircular π system may be greatly affected by adjacent nuclei residing above and below the ligand plane.

3.2. Reactivity of {nn(PM)(PI)}FeL_n. **3.2.1. Attempts at Oxidative Addition.** Little has been reported about transformations of {nn(PM)(PI)}FeL_n for good reason; there is a lack of substantive, clean reactivity. Attempts to withdraw the electrons from the {nn(PM)(PI)}²⁻ ligand in 2-(PMe₃)₂ with oxidants such as I₂, Br₂, or MeI led to degradation, as did efforts to effect NR or CR₂ transfer from RN₃ or RR'CHN₂ [RR'C = Ph₂C, (TMS)HC, etc.]. Similar negative results were obtained for 3-PMe₃, although treatment of 3-CO with MeI afforded an insoluble yellow product that exhibited a $\nu(\text{CO})$ of 1942 cm⁻¹. While the formation of [{nn(PM)(PI)}Fe(Me)CO]I [4-(Me)CO] seemed plausible, failure to generate a soluble species via counterion exchange, and the absence of a related product from longer-chain RI, rendered its formulation tentative at best.

3.2.2. Rationale for Degradative Reactivity. In the above attempts to extract electrons from the {nn(PM)(PI)}²⁻ ligand, thereby expanding the oxidative capability of the iron centers, degradation was observed. It must be noted that the only {nn(PM)(PI)}ⁿ ($n = 0$) ligated species reported is the dication 2²⁺-(PMe₃)₂, whose relative insolubility and electronic saturation via its 18e⁻ configuration are probably key to its apparent stability. It is plausible that the instability of the neutral {nn(PM)(PI)}⁰ ligand prevents these systems from utilizing the redox noninnocent character in situations of

Scheme 5



chemical reactivity. Furthermore, no radical coupling reactions were identified in the oxidation attempts, and any such compounds are likely to have limited solubility and may be part of the solid degradation products. It has been noted in a related nickel system⁷² that delocalization of the electron density can severely attenuate radical reactivity.

3.3. How Does RNI Support Chemical Reactivity?

Ligand RNI is a phenomenon that can extend capabilities of metals that are less likely to manifest multioxidation state chemistry.^{5–15} As a consequence, the most interesting applications of redox-active ligands thus far are in the first row of the transition elements, where common oxidation states are more limited than those in the second or third row,^{77–82} and in early-transition-metal chemistry, where high oxidation states dominate.^{83–88}

Scheme 5 illustrates two recent examples of how RNI appears to enable chemistry that may not be possible with more conventional examples. Heyduk et al. have placed RNI triamides about Zr^{IV} and Ta^V such that they can reduce the metal center, thereby allowing the formation of M=NR (=Y) via oxidation of the ligand.^{83,84} In its reduced state, the ligand has an 18e⁻ π system whereby the two rings are coupled by an amide lone pair. In its oxidized state, the ligand is intrinsically unstable as a 4n π system (16e⁻),⁹² but because it is chelated to a d⁰ metal center, it is stabilized with respect to metal redox chemistry. Transfer of the M=NR group can occur subsequently to regenerate the ligand in its 4n + 2 (18e⁻)⁹² state.

Another recent set of examples provided by Chirik et al. showcase the 2,6-pyridinediimine (PDI) ligand, one of which is illustrated in Scheme 5.^{77–81} In these cases, the RNI capability of PDI operates in the reverse of the prior example. The 10e⁻ π system of the neutral (i.e., oxidized) ligand is reduced to the 12e⁻ diradical dianion in stabilizing the iron as Fe^{II}, but the stability of the former abets a formal oxidative addition at the metal center that enables a catalytic ene-yne coupling. While the ligand redox processes cannot be *proven* in this case, there is ample physical characterization of the complexes that is consistent with the RNI capability of PDI. Note that the “unstable” 4n-reduced⁹² PDI²⁻ ligand is stabilized through the electrostatics of binding to the ferrous center.

It is likely that the ligand reported herein, {nn(PM)(PI)}ⁿ, while exhibiting RNI, is not capable of operating in the correct sense to aid in simple oxidative processes in the first row. In simplest terms, the 14e⁻ dianion form is too stable as a 4n + 2 species electrostatically stabilized by the ferrous center, and its oxidized/neutral form is too unstable as a 4n π system adjacent to a reductant, i.e., Fe⁰. Consider the hypothetical oxidative addition of X₂ to {nn(PM)(PI)}FeL to form {nn(PM)(PI)}-FeX₂ and L. Here it must be the situation that the ferrous center is incapable of stabilizing the oxidized {nn(PM)(PI)}⁰ ligand to the extent necessary for productive chemistry. Facile ligand degradation may occur at the ferrous center or {nn(PM)(PI)}⁰ may even be able to access Fe^{III} under reaction conditions, thereby promoting other destructive pathways. There is some evidence that related ligand capabilities can lead to C–C bond formation, and this will be explored in due course.

Why does {nn(PM)(PI)}ⁿ fail for first-row chemistry while the amide-dianilide utilized by Heyduk is successful for early-transition-metal second- and third-row transformations? Both incur the same 4n + 2 \rightarrow 4n changes⁹² in setting up the metal center for oxidative processes. Both are most stable in their reduced state and electrostatically stabilized by the charged metal center to which they are bound, while their oxidized states are intrinsically unstable when they are bound to reduced metal centers. The difference is in the oxidation process itself. The capture of a nitrene by the early-transition-metal centers ensures that the metal center, a d⁰ Ta^V or Zr^{IV}, has roughly the same ligand set in terms of nitrogen donors: two nitrogen lone-pair donors and an amide from the oxidized chelate and an imido group versus the initial triamide. In the case of {nn(PM)(PI)}ⁿ, the formation of an Fe=NR group (or FeX₂, etc.) at a d⁶ metal center cannot adequately compensate for the loss of the dianionic chelate, and the possibility of accessing Fe^{III} renders oxidative processes at {nn(PM)(PI)}-FeL highly problematic.

4. CONCLUSIONS

A nacnac ligand has been successfully implemented as a component of a tetradentate chelate in the form of {nn(PM)₂}FeX (1-X; X = N(TMS)₂, Cl, N₃) and as part of a redox

noninnocent ligand in $\{\text{nn}(\text{PM})(\text{PI})\}\text{FeL}$ (3-L; L = CO, PMe_3 , PMePh_2 , PPh_3) and $\{\text{nn}(\text{PM})(\text{PI})\}\text{FeLL}'$ [2-L,L'; L,L' = PMe_3 , PMe_2Ph , and $\text{PMe}_3(\text{CO})$]. In 2-L,L' and 3-L, $\{\text{nn}(\text{PM})(\text{PI})\}^{2-}$ is a dianionic ligand that effectively stabilizes Fe^{II} and provides a strong-field environment that renders the compounds diamagnetic. Computational studies indicate a strong degree of covalency to these species and support the structural and spectroscopic observations that successive $1e^-$ oxidations of 2-(PMe_3)₂ occur at the ligand. While the lack of consequential reactivity to 2-L,L' and 3-L was disappointing, analysis of the results has permitted an initial, fundamental view of what is necessary for RNI to play a role in catalysis, in particular the role of earth-abundant first-row transition metals as precious metal surrogates.

5. EXPERIMENTAL SECTION

5.1. General Considerations. The full experimental details have been deposited as SI, so that the actual spectra may be presented for complexes in which elemental analyses varied outside of the generally accepted ranges.

■ ASSOCIATED CONTENT

Supporting Information

X-ray crystallographic data in CIF format, MB spectra pertaining to 2^+ -(PMe_3)₂ and 2^{2+} -(PMe_3)₂, comments related to the structure of 2^{2+} -(PMe_3)₂, and full experimental details, including original NMR spectra. This material is available free of charge via the Internet at <http://pubs.acs.org>.

■ AUTHOR INFORMATION

Corresponding Author

*E-mail: ptw2@cornell.edu. Fax: 607 255 4173.

Notes

The authors declare no competing financial interest.

■ ACKNOWLEDGMENTS

P.T.W. thanks the NSF (Grant CHE-1055505) and Cornell University and T.R.C. the NSF (Grant CHE-1057758) for financial support.

■ REFERENCES

- (1) Frazier, B. A.; Wolczanski, P. T.; Lobkovsky, E. B. *Inorg. Chem.* **2009**, *48*, 11576–11585.
- (2) Frazier, B. A.; Bartholomew, E. R.; Wolczanski, P. T.; DeBeer, S.; Santiago-Berrios, M.; Abruña, H. D.; Lobkovsky, E. B.; Bart, S. C.; Mossin, S.; Meyer, K.; Cundari, T. R. *Inorg. Chem.* **2011**, *50*, 12414–12436.
- (3) Frazier, B. A.; Wolczanski, P. T.; Lobkovsky, E. B.; Cundari, T. R. *J. Am. Chem. Soc.* **2009**, *131*, 3428–3429.
- (4) Hulley, E. B.; Wolczanski, P. T.; Lobkovsky, E. B. *J. Am. Chem. Soc.* **2011**, *133*, 18058–18061.
- (5) Frazier, B. A.; Wolczanski, P. T.; Keresztes, I.; DeBeer, S.; Lobkovsky, E. B.; Pierpont, A. W.; Cundari, T. R. *Inorg. Chem.* **2012**, *51*, 8177–8186.
- (6) Frazier, B. A.; Williams, V. A.; Wolczanski, P. T.; Bart, S.; Meyer, K.; Cundari, T. R.; Lobkovsky, E. B. *Inorg. Chem.* **2013**, *52*, 3295–3312.
- (7) Jørgensen, C. K. *Helv. Chim. Acta* **1967**, *50* (Supp. 1), 131–146.
- (8) Pierpont, C. G. *Coord. Chem. Rev.* **2001**, *216*, 99–125.
- (9) Evangelio, E.; Ruiz-Molina, D. *Eur. J. Inorg. Chem.* **2005**, 2957–2971.
- (10) Ray, K.; Petrenko, T.; Wiegardt, K.; Neese, F. *Dalton Trans.* **2007**, 1552–1566.
- (11) (a) De Bruin, B.; Hettterscheid, D. G. H.; Koekkoek, A. J. J.; Grutzmacher, H. *Prog. Inorg. Chem.* **2007**, *55*, 247–354. (b) Dzik, W.

L.; van der Vlugt, J. I.; Reek, J. N. H.; de Bruin, B. *Angew. Chem., Int. Ed.* **2011**, *50*, 3356–3358.

- (12) Blanchard, S.; Derat, E.; Desage-El Murr, M.; Fensterbank, L.; Malacria, M.; Mouries-Mansuy, V. *Eur. J. Inorg. Chem.* **2012**, 376–389.
- (13) Caulton, K. G. *Eur. J. Inorg. Chem.* **2012**, 435–443.
- (14) Budzelaar, P. H. M. *Eur. J. Inorg. Chem.* **2012**, 530–534.
- (15) Jiao, R.; Shen, X. D.; Xue, M. Q.; Zhang, Y.; Yao, Y. M.; Shen, Q. *Chem. Commun.* **2010**, 46, 4118–4120.
- (16) Holland, P. L. *Acc. Chem. Res.* **2008**, *41*, 905–914.
- (17) (a) Smith, J. M.; Sadique, A. R.; Cundari, T. R.; Rodgers, K. R.; Lakat-Rodgers, G.; Lachicotte, R. J.; Flaschenriem, C. J.; Vela, J.; Holland, P. L. *J. Am. Chem. Soc.* **2006**, *128*, 756–769. (b) Smith, J. M.; Lachicotte, R. J.; Pittard, K. A.; Cundari, T. R.; Lukat-Rodgers, G.; Rodgers, K. R.; Holland, P. L. *J. Am. Chem. Soc.* **2001**, *123*, 9222–9223.
- (18) (a) Holland, P. L.; Cundari, T. R.; Perez, L. L.; Eckert, N. A.; Lachicotte, R. J. *J. Am. Chem. Soc.* **2002**, *124*, 14416–14424. (b) Andres, H.; Bominaar, E. L.; Smith, J. M.; Eckert, N. A.; Holland, P. L.; Munk, E. J. *J. Am. Chem. Soc.* **2002**, *124*, 3012–3025.
- (19) (a) Cowley, R. E.; Eckert, N. A.; Vaddadi, S.; Figg, T. M.; Cundari, T. R.; Holland, P. L. *J. Am. Chem. Soc.* **2011**, *133*, 9796–9811. (b) Eckert, N. A.; Vaddadi, S.; Stoian, S.; Lachicotte, R. J.; Cundari, T. R.; Holland, P. L. *Angew. Chem., Int. Ed.* **2006**, *45*, 6868–6871. (c) Cowley, R. E.; Holland, P. L. *Inorg. Chem.* **2012**, *51*, 8352–8361.
- (20) Yu, Y.; Sadique, A. R.; Smith, J. M.; Dugan, T. R.; Cowley, R. E.; Brennessel, W. W.; Flaschenriem, C. J.; Bill, E.; Cundari, T. R.; Holland, P. L. *J. Am. Chem. Soc.* **2008**, *130*, 6624–6638.
- (21) (a) Vela, J.; Smith, J. M.; Yu, Y.; Ketterer, N. A.; Flaschenriem, C. J.; Lachicotte, R. J.; Holland, P. L. *J. Am. Chem. Soc.* **2005**, *127*, 7857–7870. (b) Dugan, T. R.; Goldberg, J. M.; Brennessel, W. W.; Holland, P. L. *Organometallics* **2012**, *31*, 1349–1360.
- (22) (a) Dugan, T. R.; Bill, E.; MacLeod, K. C.; Christian, G. J.; Cowley, R. E.; Brennessel, W. W.; Ye, S. F.; Neese, F.; Holland, P. L. *J. Am. Chem. Soc.* **2012**, *134*, 20352–20364. (b) Cowley, R. E.; Golder, M. R.; Eckert, N. A.; Al-Afyouni, M. H.; Holland, P. L. *Organometallics* **2013**, *32*, 5289–5298.
- (23) (a) Rodriguez, M. M.; Bill, E.; Brennessel, W. W.; Holland, P. L. *Science* **2011**, *334*, 780–783. (b) Chiang, K. P.; Bellows, S. M.; Brennessel, W. W.; Holland, P. L. *Chem. Sci.* **2014**, *5*, 267–274.
- (24) (a) Wiese, S.; McAfee, J. L.; Pahls, D. R.; McMullin, C. L.; Cundari, T. R.; Warren, T. H. *J. Am. Chem. Soc.* **2012**, *134*, 10114–10121. (b) Kogut, E.; Wiencko, H. L.; Zhang, L. B.; Cordeau, D. E.; Warren, T. J. *J. Am. Chem. Soc.* **2005**, *127*, 11248–11249. (c) Kogut, E.; Zeller, A.; Warren, T. H.; Strassner, T. *J. Am. Chem. Soc.* **2004**, *126*, 11984–11994.
- (25) (a) Gephart, R. T.; Huang, D. L.; Aguila, M. J. B.; Schmidt, G.; Shahu, A.; Warren, T. H. *Angew. Chem., Int. Ed.* **2012**, *51*, 6488–6492. (b) Badei, Y. M.; Krishnaswamy, A.; Melzer, M. M.; Warren, T. H. *J. Am. Chem. Soc.* **2006**, *128*, 15056–15057. (c) Dai, X. L.; Warren, T. H. *J. Am. Chem. Soc.* **2004**, *126*, 10085–10094. (d) Gephart, R. T.; McMullin, C. L.; Sapiezynski, N. G.; Jang, E. S.; Aguila, M. J. B.; Cundari, T. R.; Warren, T. H. *J. Am. Chem. Soc.* **2012**, *134*, 17350–17353.
- (26) Dai, X. L.; Kapoor, P.; Warren, T. H. *J. Am. Chem. Soc.* **2004**, *126*, 4798–4799.
- (27) Mindiola, D. J. *Acc. Chem. Res.* **2006**, *39*, 813–821.
- (28) Mindiola, D. J. *Angew. Chem., Int. Ed.* **2009**, *48*, 6198–6200.
- (29) (a) Tran, B. L.; Washington, M. P.; Henckel, D. A.; Gao, X. F.; Park, H.; Pink, M.; Mindiola, D. J. *Chem. Commun.* **2012**, 1529–1531. (b) Bailey, B. C.; Basuli, F.; Huffman, J. C.; Mindiola, D. J. *Organometallics* **2006**, *25*, 3963–3968. (c) Kilgore, U. J.; Basuli, F.; Huffman, J. C.; Mindiola, D. J. *Inorg. Chem.* **2006**, *45*, 487–489. (d) Basuli, F.; Aneetha, H.; Huffman, J. C.; Mindiola, D. J. *J. Am. Chem. Soc.* **2005**, *127*, 17992–17993. (e) Zhao, G. Y.; Basuli, F.; Kilgore, U. J.; Fan, H. J.; Aneetha, H.; Huffman, J. C.; Wu, G.; Mindiola, D. J. *J. Am. Chem. Soc.* **2006**, *128*, 13575–13585.
- (30) Adhikari, D.; Basuli, F.; Orlando, J. H.; Gao, X. F.; Huffman, J. C.; Pink, M.; Mindiola, D. J. *Organometallics* **2009**, *28*, 4115–4125.

- (31) (a) Tran, B. L.; Singhal, M.; Park, H.; Lam, O. P.; Pink, M.; Krzystek, J.; Ozarowski, A.; Telsler, J.; Meyer, K.; Mindiola, D. J. *Angew. Chem., Int. Ed.* **2010**, *49*, 9871–9875. (b) Tran, B. L.; Pinter, B.; Nichols, A. J.; Konopka, F. T.; Thompson, R.; Chen, C. H.; Krzystek, J.; Ozarowski, A.; Telsler, J.; Baik, M. H.; Meyer, K.; Mindiola, D. J. *J. Am. Chem. Soc.* **2012**, *134*, 13035–13045.
- (32) Fan, H. J.; Adhikari, D.; Saleh, A. A.; Clark, R. L.; Zuno-Cruz, F. J.; Cabrera, G. S.; Huffman, J. C.; Pink, M.; Mindiola, D. J.; Baik, M. H. *J. Am. Chem. Soc.* **2008**, *130*, 17351–17361.
- (33) MacAdams, L. A.; Kim, W. K.; Liable-Sands, L. M.; Guzei, I. A.; Rheingold, A. L.; Theopold, K. H. *Organometallics* **2002**, *21*, 952–960.
- (34) (a) Kim, W. K.; Fevola, M. J.; Liable-Sands, L. M.; Rheingold, A. L.; Theopold, K. H. *Organometallics* **1998**, *17*, 4541–4543. (b) MacAdams, L. A.; Buffone, G. P.; Incarvito, C. D.; Rheingold, A. L. *J. Am. Chem. Soc.* **2005**, *127*, 1082–1083. (c) Monillas, W. H.; Young, J. F.; Yap, G. P. A.; Theopold, K. H. *Dalton Trans.* **2013**, *42*, 9198–9210.
- (35) (a) Monillas, W. H.; Yap, G. P. A.; MacAdams, L. A.; Theopold, K. H. *J. Am. Chem. Soc.* **2007**, *129*, 8090–8091. (b) Dai, F.; Yap, G. P. A.; Theopold, K. H. *J. Am. Chem. Soc.* **2013**, *135*, 16774–16776. (c) Monillas, W. H.; Yap, G. P. A.; Theopold, K. H. *Inorg. Chim. Acta* **2011**, *369*, 103–119.
- (36) (a) Monillas, W. H.; Yap, G. P. A.; Theopold, K. H. *Angew. Chem., Int. Ed.* **2007**, *46*, 6692–6694. (b) Benard, M.; Rohmer, M. M.; Lopez, X.; Theopold, K. H. *Angew. Chem., Int. Ed.* **2008**, *47*, 5597–5599. (c) MacAdams, L. A.; Buffone, G. P.; Incarvito, C. D.; Golen, J. A.; Rheingold, A. L.; Theopold, K. H. *Chem. Commun.* **2003**, 1164–1165.
- (37) Whitehorne, T. J. J.; Schaper, F. *Inorg. Chem.* **2013**, *52*, 13612–13622.
- (38) Gupta, A. K.; Tolman, W. B. *Inorg. Chem.* **2012**, *51*, 1881–1888.
- (39) (a) Chang, K. C.; Lu, C. F.; Wang, P. Y.; Lu, D. Y.; Chen, H. Z.; Kuo, T. S.; Tsai, Y. C. *Dalton Trans.* **2011**, *40*, 2324–2331. (b) Lin, K. M.; Wang, P. Y.; Shieh, Y. J.; Chen, H. Z.; Kuo, T. S.; Tsai, Y. C. *New J. Chem.* **2010**, *34*, 1737–1745.
- (40) Tonzetich, Z. J.; Heroquel, F.; Do, L. H.; Lippard, S. J. *Inorg. Chem.* **2011**, *50*, 1570–1579.
- (41) (a) Zhou, W.; Tang, L. M.; Patrick, B. O.; Smith, K. M. *Organometallics* **2011**, *30*, 603–610. (b) Chapouret, Y.; MacLeod, K. C.; Baisch, U.; Patrick, B. O.; Smith, K. M.; Poli, R. *Organometallics* **2010**, *29*, 167–176.
- (42) El-Zoghbi, L.; Kebdani, M.; Whitehorne, T. J. J.; Schaper, F. *Organometallics* **2013**, *32*, 6986–6995.
- (43) (a) Gianetti, T. L.; Nocton, S. G.; Minasian, S. G.; Tomson, N. C.; Kilcoyne, A. L. D.; Kozimor, S. A.; Shuh, D. K.; Tyliczszak, T.; Bergman, R. G.; Arnold, J. *J. Am. Chem. Soc.* **2013**, *135*, 3224–3236. (b) Gianetti, T. L.; Bergman, R. G.; Arnold, J. *J. Am. Chem. Soc.* **2013**, *135*, 8145–8148. (c) Gianetti, T. L.; Tomson, N. C.; Arnold, J.; Bergman, R. G. *J. Am. Chem. Soc.* **2011**, *133*, 14904–14907. (d) Tomson, N. C.; Arnold, J.; Bergman, R. G. *Organometallics* **2010**, *29*, 5010–5025. (e) Tomson, N. C.; Arnold, J.; Bergman, R. G. *Organometallics* **2010**, *29*, 2926–2942. (f) Tomson, N. C.; Arnold, J.; Bergman, R. G. *Dalton Trans.* **2011**, *40*, 7718–7729.
- (44) (a) Hadzovic, A.; Song, D. T. *Inorg. Chem.* **2008**, *47*, 12010–12017. (b) Annibale, V. T.; Tan, R. Y.; Janetzko, J.; Lund, L. M.; Song, D. T. *Inorg. Chim. Acta* **2012**, *380*, 308–321.
- (45) (a) Phillips, A. D.; Thommes, K.; Scopelliti, R.; Gandolfi, C.; Albrecht, M.; Severin, K.; Schreiber, D. F.; Dyson, P. J. *Organometallics* **2011**, *30*, 6119–6132. (b) Phillips, A. D.; Zava, O.; Scopelliti, R.; Nazarov, A. A.; Dyson, P. J. *Organometallics* **2010**, *29*, 417–427.
- (46) Tsai, Y. C. *Coord. Chem. Rev.* **2012**, *256*, 722–758.
- (47) Yao, S. L.; Driess, M. *Acc. Chem. Res.* **2012**, *45*, 276–287.
- (48) Marshak, M. P.; Chambers, M. B.; Nocera, D. G. *Inorg. Chem.* **2012**, *51*, 11190–11197.
- (49) Khusniyarov, M. M.; Bill, E.; Weyhermüller, T.; Bothe, E.; Wieghardt, K. *Angew. Chem., Int. Ed.* **2011**, *50*, 1652–1655.
- (50) (a) Hope, J. M.; Wilson, J. J.; Lippard, S. J. *Dalton Trans.* **2013**, *42*, 3176–3180. (b) Marlier, E. E.; Sadowsky, D.; Cramer, C. J.; McNeill, K. *Inorg. Chim. Acta* **2011**, *369*, 173–179.
- (51) Marlier, E. E.; Ulrich, B. A.; McNeill, K. *Inorg. Chem.* **2012**, *51*, 2079–2085.
- (52) (a) Olmstead, M. M.; Power, P. P.; Shoner, S. C. *Inorg. Chem.* **1991**, *30*, 2547–2551. (b) Andersen, R. A.; Faegri, K.; Green, J. C.; Haaland, A.; Lappert, M. F.; Leung, W. P.; Rypdal, K. *Inorg. Chem.* **1988**, *27*, 1782–1786.
- (53) (a) Evans, D. F. *J. Chem. Soc.* **1959**, 2003–2005. (b) Schubert, E. M. *J. Chem. Educ.* **1992**, *69*, 62.
- (54) Carlin, R. L. *Magnetochemistry*; Springer-Verlag: Berlin, 1986.
- (55) Figgis, B. N.; Hitchman, M. A. *Ligand Field Theory and Its Applications*; Wiley-VCH: New York, 2000.
- (56) Parish, R. V. *NMR, NQR, EPR, and Mössbauer Spectroscopy in Inorganic Chemistry*; Ellis Horwood: West Sussex, England, 1990.
- (57) Gütlisch, P.; Bill, E.; Trautwein, A. X. *Mössbauer Spectroscopy and Transition Metal Chemistry*; Springer: New York, 2011.
- (58) Fultz, B. *Mössbauer Spectrometry*. In *Characterization of Materials*; Kaufmann, E., Ed.; John Wiley: New York, 2011.
- (59) Addison, A. W.; Rao, T. N.; Reedijk, J.; van Rijn, J.; Verschoor, G. C. *J. Chem. Soc., Dalton Trans.* **1984**, 1349–1356.
- (60) Buschmann, W. E.; Miller, J. S. *Inorg. Synth.* **2002**, *33*, 83–91.
- (61) (a) Vasudev, P.; Jones, C. H. W. *Can. J. Chem.* **1973**, *51*, 405–410. (b) Collins, R. L.; Pettit, R. *J. Chem. Phys.* **1963**, *39*, 3433–3436. (c) Dias, G. H. M.; Morigaki, M. K. *Polyhedron* **1992**, *11*, 1629–1636.
- (62) Volpe, E. C.; Wolczanski, P. T.; Darmon, J. M.; Lobkovsky, E. B. *Polyhedron* **2013**, *52*, 406–415.
- (63) (a) Lee, Y.; Mankad, N. P.; Peters, J. C. *Nat. Chem.* **2010**, *2*, 558–565. (b) Heinrich, M. P.; Gunderson, W.; Behan, R. K.; Green, M. T.; Mehn, M. P.; Betley, T. A.; Lu, C. C.; Peters, J. C. *Proc. Natl. Acad. Sci. U.S.A.* **2006**, *46*, 17107–17112.
- (64) Chlopek, K.; Bill, E.; Weyhermüller, T.; Wieghardt, K. *Inorg. Chem.* **2005**, *44*, 7087–7089.
- (65) Bart, S. C.; Chlopek, K.; Bill, E.; Bouwkamp, M. W.; Lobkovsky, E.; Neese, F.; Wieghardt, K.; Chirik, P. J. *J. Am. Chem. Soc.* **2006**, *128*, 13901–13912.
- (66) Thammavongsy, Z.; Seda, T.; Zakharov, L. N.; Kaminsky, W.; Gilbertson, J. D. *Inorg. Chem.* **2012**, *51*, 9168–9170.
- (67) (a) Therien, M. J.; Trogler, W. C. *J. Am. Chem. Soc.* **1986**, *108*, 3697–3702. (b) MacNeil, J. H.; Chiverton, A. C.; Fortier, S.; Baird, M. C.; Hynes, R. C.; Williams, A. J.; Preston, K. F.; Ziegler, T. *J. Am. Chem. Soc.* **1991**, *113*, 9834–9842.
- (68) Baird, M. C. *Chem. Rev.* **1988**, *88*, 1217–1227.
- (69) (a) Mankad, N. P.; Whited, M. T.; Peters, J. C. *Angew. Chem., Int. Ed.* **2007**, *46*, 5768–5771. (b) Lee, Y.; Kinney, R. A.; Hoffman, B. M.; Peters, J. C. *J. Am. Chem. Soc.* **2011**, *133*, 16366–16369.
- (70) Allen, F. H.; Kennard, O.; Watson, D. G.; Brammer, L.; Orpen, A. G.; Taylor, R. *J. Chem. Soc., Perkin Trans. 2* **1987**, S1–S19.
- (71) (a) Lu, C. C.; Bill, E.; Weyhermüller, T.; Bothe, E.; Wieghardt, K. *J. Am. Chem. Soc.* **2008**, *130*, 3181–3197. (b) Lu, C. C.; Weyhermüller, T.; Bill, E.; Wieghardt, K. *Inorg. Chem.* **2009**, *48*, 6055–6064.
- (72) Williams, V. A.; Hulley, E. B.; Wolczanski, P. T.; Lancaster, K. M.; Lobkovsky, E. B. *Chem. Sci.* **2013**, *4*, 3636–3648.
- (73) (a) Stieber, S. C. E.; Milsman, C.; Hoyt, J. M.; Turner, Z. R.; Finkelstein, K. D.; Wieghardt, K.; DeBeer, S.; Chirik, P. J. *Inorg. Chem.* **2012**, *51*, 3770–3785. (b) Russell, S. K.; Bowman, A. C.; Lobkovsky, E.; Wieghardt, K.; Chirik, P. J. *Eur. J. Inorg. Chem.* **2012**, 535–545. (c) Bowman, A. C.; Milsman, C.; Bill, E.; Lobkovsky, E.; Weyhermüller, T.; Wieghardt, K.; Chirik, P. J. *Inorg. Chem.* **2010**, *49*, 6110–6123. (d) Bowman, A. C.; Milsman, C.; Atienza, C. C. H.; Lobkovsky, E.; Wieghardt, K.; Chirik, P. J. *J. Am. Chem. Soc.* **2010**, *132*, 1676–1684. (e) Wile, B. M.; Trovitch, R. J.; Bart, S. C.; Tondreau, A. M.; Lobkovsky, E. B.; Milsman, C.; Bill, E.; Wieghardt, K.; Chirik, P. J. *Inorg. Chem.* **2009**, *48*, 4190–4200.
- (74) (a) Volpe, E. C.; Wolczanski, P. T.; Lobkovsky, E. B. *Organometallics* **2010**, *29*, 364–377. (b) Bartholomew, E. R.; Volpe, E. C.; Wolczanski, P. T.; Lobkovsky, E. B.; Cundari, T. R. *J. Am. Chem. Soc.* **2013**, *135*, 3511–3527.
- (75) (a) Chlopek, K.; Muresan, N.; Neese, F.; Wieghardt, K. *Chem.—Eur. J.* **2007**, *13*, 8391–8403. (b) Ghosh, P.; Bill, E.;

Weyhermüller, T.; Neese, F.; Wieghardt, K. *J. Am. Chem. Soc.* **2004**, *125*, 1293–1308.

(76) Neese, F. *J. Phys. Chem. Solids* **2004**, *65*, 781–785.

(77) (a) Hoyt, J. M.; Sylvester, K. T.; Semproni, S. P.; Chirik, P. J. *J. Am. Chem. Soc.* **2013**, *135*, 4862–4877. (b) Sylvester, K. T.; Chirik, P. J. *J. Am. Chem. Soc.* **2009**, *131*, 8772–8773. (c) Bouwkamp, M. W.; Bowman, A. C.; Lobkovsky, E.; Chirik, P. J. *J. Am. Chem. Soc.* **2006**, *128*, 13340–13341.

(78) Russell, S. K.; Lobkovsky, E.; Chirik, P. J. *J. Am. Chem. Soc.* **2011**, *133*, 8858–8861.

(79) Darmon, J. M.; Stieber, S. C.; Sylvester, K. L.; Fernández, I.; Lobkovsky, E.; Semproni, S. P.; Bill, E.; Wieghardt, K.; DeBeer, S.; Chirik, P. J. *J. Am. Chem. Soc.* **2012**, *134*, 17125–17137.

(80) (a) Monfette, S.; Turner, Z. R.; Semproni, S. P.; Chirik, P. J. *J. Am. Chem. Soc.* **2012**, *134*, 4561–4564. (b) Yu, R. P.; Darmon, J. M.; Hoyt, H. M.; Margulieux, G. W.; Turner, Z.; Chirik, P. J. *ACS Catal.* **2012**, *2*, 1760–1764. (c) Trovitch, R. J.; Lobkovsky, E.; Bill, E.; Chirik, P. J. *Organometallics* **2008**, *27*, 1470–1478. (d) Bart, S. C.; Lobkovsky, E.; Chirik, P. J. *J. Am. Chem. Soc.* **2004**, *126*, 13794–13807.

(81) (a) Tondreau, A. M.; Atienza, C. C. H. A.; Weller, K. J.; Nye, S. A.; Lewis, K. M.; Delis, J. G. P.; Chirik, P. J. *Science* **2012**, *335*, 567–570. (b) Tondreau, A. M.; Atienza, C. C. H. A.; Darmon, J. M.; Milsmann, C.; Hoyt, H. M.; Weller, K. J.; Nye, S. A.; Lewis, K. N.; Boyer, J.; Delis, J. G. P.; Lobkovsky, E.; Chirik, P. J. *Organometallics* **2012**, *4886*–4893. (c) Atienza, C. C. H. A.; Tondreau, A. M.; Weller, K. J.; Lewis, K. M.; Cruse, R.; Nye, S. A.; Boyer, J. L.; Delis, J. P.; Chirik, P. J. *ACS Catal.* **2012**, *2*, 2169–2172. (d) Tondreau, A. M.; Lobkovsky, E.; Chirik, P. J. *Org. Lett.* **2008**, *10*, 2789–2792. (e) Tondreau, A. M.; Darmon, J. D.; Wile, B. M.; Floyd, S. K.; Lobkovsky, E. B.; Chirik, P. J. *Organometallics* **2009**, *28*, 3928–3940.

(82) Karpinić, S. S.; McGuinness, D. S.; Britovsek, G. J. P.; Patel, J. *Organometallics* **2012**, *31*, 3439–3442.

(83) Heyduk, A. F.; Zarkesh, R. A.; Nguyen, A. I. *Inorg. Chem.* **2011**, *50*, 9849–9863.

(84) (a) Blackmore, K. J.; Lal, N.; Ziller, J. W.; Heyduk, A. F. *J. Am. Chem. Soc.* **2008**, *130*, 2728–2729. (b) Nguyen, A. I.; Zarkesh, R. A.; Lacy, D. C.; Thorson, M. K.; Heyduk, A. F. *Chem. Sci.* **2011**, *2*, 166–169. (c) Blackmore, K. J.; Ziller, J. W.; Heyduk, A. F. *Inorg. Chem.* **2005**, *44*, 5559–5561. (d) Zarkesh, R. A.; Ziller, J. W.; Heyduk, A. F. *Angew. Chem., Int. Ed.* **2008**, *47*, 4715–4718. (e) Haneline, M. R.; Heyduk, A. F. *J. Am. Chem. Soc.* **2006**, *128*, 8410–8411.

(85) Ketterer, N. A.; Fan, H.; Blackmore, K. J.; Yang, X.; Ziller, J. W.; Baik, M.-H.; Heyduk, A. F. *J. Am. Chem. Soc.* **2008**, *130*, 4364–4374.

(86) Marshall-Roth, T.; Liebscher, S. C.; Rickert, K.; Seewald, N. J.; Oliver, A. G.; Brown, S. N. *Chem. Commun.* **2012**, *48*, 7826–7828.

(87) Corneliu, S.; Jones, M. E.; Fanwick, P. E.; Abu-Omar, M. M. *J. Am. Chem. Soc.* **2007**, *129*, 12400–12401; *J. Am. Chem. Soc.* **2007**, *129*, 12400–12401.

(88) (a) Smith, A. L.; Hardcastle, K. I.; Soper, J. D. *J. Am. Chem. Soc.* **2010**, *132*, 14358–14360. (b) Lippert, C. A.; Arnstein, S. A.; Sherrill, C. D.; Soper, J. D. *J. Am. Chem. Soc.* **2010**, *132*, 3879–3892. (c) Rolle, C. J., III; Hardcastle, K. I.; Soper, J. D. *Inorg. Chem.* **2008**, *47*, 1892–1894.

(89) Sinnecker, S.; Neese, F. *J. Phys. Chem. A* **2006**, *110*, 12267–12275.

(90) Orío, M.; Pantazis, D. A.; Petrenko, T.; Neese, F. *Inorg. Chem.* **2009**, *48*, 7251–7260.

(91) Neese, F. *J. Phys. Chem. A* **2001**, *105*, 4290–4299.

(92) Goldstein, M.; Hoffmann, R. *J. Am. Chem. Soc.* **1971**, *93*, 6193–6204.

(93) Zhao, Y.; Truhlar, D. G. *Acc. Chem. Res.* **2008**, *41*, 157–167.

(94) Krishnan, R.; Binkley, J. S.; Seeger, R.; Pople, J. A. *J. Chem. Phys.* **1980**, *72*, 650–654.

(95) Frisch, M. J.; Trucks, G. W.; Schlegel, H. B.; Scuseria, G. E.; Robb, M. A.; Cheeseman, J. R.; Scalmani, G.; Barone, V.; Mennucci, B.; Petersson, G. A.; Nakatsuji, H.; Caricato, M.; Li, X.; Hratchian, H. P.; Izmaylov, A. F.; Bloino, J.; Zheng, G.; Sonnenberg, J. L.; Hada, M.; Ehara, M.; Toyota, K.; Fukuda, R.; Hasegawa, J.; Ishida, M.; Nakajima, T.; Honda, Y.; Kitao, O.; Nakai, H.; Vreven, T.; Montgomery, J. A., Jr.

Peralta, J. E.; Ogliaro, F.; Bearpark, M.; Heyd, J. J.; Brothers, E.; Kudin, K. N.; Staroverov, V. N.; Kobayashi, R.; Normand, J.; Raghavachari, K.; Rendell, A.; Burant, J. C.; Iyengar, S. S.; Tomasi, J.; Cossi, M.; Rega, N.; Millam, J. M.; Klene, M.; Knox, J. E.; Cross, J. B.; Bakken, V.; Adamo, C.; Jaramillo, J.; Gomperts, R.; Stratmann, R. E.; Yazyev, O.; Austin, A. J.; Cammi, R.; Pomelli, C.; Ochterski, J. W.; Martin, R. L.; Morokuma, K.; Zakrzewski, V. G.; Voth, G. A.; Salvador, P.; Dannenberg, J. J.; Dapprich, S.; Daniels, A. D.; Farkas, Ö.; Foresman, J. B.; Ortiz, J. V.; Cioslowski, J.; Fox, D. J. *Gaussian 09*, revision A.1; Gaussian, Inc.: Wallingford, CT, 2009.